Physica D 432 (2022) 133136

Contents lists available at ScienceDirect

Physica D

journal homepage: www.elsevier.com/locate/physd

On the Sun-shadow dynamics

Irene Cavallari[1,*], Giovanni F. Gronchi[2], Giulio Baù[3]

Dipartimento di Matematica, Università di Pisa, Italy

ARTICLE INFO

Article history:
Received 21 November 2020
Received in revised form 30 November 2021
Accepted 16 December 2021
Available online 3 January 2022
Communicated by Gary Froyland

Keywords:
Solar radiation pressure
Patched dynamics
Periodic orbits
Section maps
Earth satellite dynamics

ABSTRACT

We investigate the planar motion of a mass particle in a force field defined by patching Kepler's and Stark's dynamics. This model is called *Sun-shadow* dynamics, referring to the motion of an Earth satellite perturbed by the solar radiation pressure and considering the Earth shadow effect. The existence of periodic orbits of brake type is proved, and the Sun-shadow dynamics is investigated by means of a Poincaré map defined by a quantity that is not conserved along the flow. We also present the results of our numerical investigations on some properties of the map. Moreover, we construct the invariant manifolds of the hyperbolic fixed points related to the periodic orbits of brake type. The global picture of the map shows evidence of regular and chaotic behaviour.

1. Introduction

This paper deals with the study of a mass particle moving under the alternated action of two different force fields: one of Kepler's problem, the other of Stark's problem, where a constant force is added to the central one. This is a basic model to study the short-period evolution of an Earth satellite which alternately spends some time in the Earth shadow and some time in the region where the solar radiation pressure acts. We call this model *Sun-shadow* dynamics.

The solar radiation pressure (srp) can become the main perturbation to be added to the monopole term of the Earth, when the *area-to-mass* ratio of the satellite is large enough. The importance of the srp for accurately predicting the motion of artificial satellites of the Earth was first shown in [1] and [2]. Musen developed an analytic theory that was applied to the Vanguard I satellite. In [2] the motions of the Echo balloons and the Beacon satellite were numerically propagated. In both works it was found that the srp can seriously affect the lifetime of an Earth satellite, especially when a particular resonance condition is satisfied. Since these pioneering studies, the effects of the srp have been investigated by many authors. For example, the long and short-period variations of the orbital elements are discussed in detail in [3].

A relevant aspect related to the srp perturbation is the passage through the Earth shadow. Kozai [4] was among the first authors to treat the eclipse perturbation and understand its effects. He developed a semi-analytic method to obtain the first-order variations of the orbital elements when the srp is switched off inside the Earth shadow. It is worth noting that, in general, the accumulation of these short-period effects produces a long-period drift of the semi-major axis, see [3]. Similarly, in [5] Lidov described a semi-analytic method to compute the secular variation of the osculating parameters. His study showed that they all oscillate periodically, except in two limiting cases in which either the argument of periapsis or both the semi-major axis and the eccentricity vary monotonically. Also Ferraz-Mello [6] studied the possible secular effects induced by the srp with the Earth shadow, by developing an analytic theory in the Hamiltonian formalism; he found that the angular drifts of the longitude, perigee, and node are quite small. A more recent paper, by Hubaux and Lemaître [7], showed that successive crossings of the shadow for long time spans (in the order of 1000 years) cause significant oscillations of the orbital elements, with amplitudes and frequencies that depend on the area-to-mass ratio. Moreover, numerical experiments carried out in [8] indicate that the passage through the shadow is a source of instability for space debris with high area-to-mass ratio at geostationary altitudes.

The idea which inspired this paper emerges in [9]. Beletsky proposed to apply Kepler's dynamics inside the Earth shadow, and Stark's dynamics outside of it. His qualitative analysis of the problem pointed out that the orbital energy has leaps each time the shadow is crossed and that the argument of periapsis, the semi-major axis and the eccentricity have long-period oscillations. More precisely, the semi-major axis decreases and the eccentricity increases while the apse line moves away from the direction of the srp force. In this work we try to go deeper into the subject. We consider the two-dimensional case where

* Corresponding author.
E-mail address: irene.cavallari@dm.unipi.it (I. Cavallari).
1 https://orcid.org/0000-0001-9541-4473
2 https://orcid.org/0000-0003-1294-0633
3 https://orcid.org/0000-0002-9857-0866

https://doi.org/10.1016/j.physd.2021.133136

the srp force lies in the plane of motion of the satellites. After reviewing Stark's dynamics following [9] and [10], we describe some features occurring when we alternate it with the dynamics of Kepler's problem, using separable variables for the Hamilton–Jacobi equations of both problems. In particular, we prove the existence of periodic orbits of brake type, i.e. orbits with zero velocity points, which are close to the unstable brake periodic orbits of Stark's dynamics. For a further description we introduce a Poincaré map $\mathfrak{S}$, that we call Sun-shadow map. For this purpose, we choose a section Σ in the boundary of the shadow region, and fix a quantity that has the same value when the section is crossed with the right orientation (but is not conserved along the flow). Then, we present the results of our numerical investigations: we describe the domain of $\mathfrak{S}$, prove that the fixed points related to the periodic orbits of brake type are hyperbolic, and compute the stable and unstable manifolds of these points. These manifolds are made of several connected components because there are orbits that either collide with the Earth or go to infinity, therefore they do not go back to Σ. Finally, a global picture of the map is drawn, showing evidence of regular and chaotic behaviour.

The paper is organised as follows. In Section 2 we introduce Kepler's and Stark's dynamics using separable coordinates for the Hamilton–Jacobi equations of the two problems. In Section 3 there is the review of Stark's problem. We investigate the alternation of the two different dynamics in Section 4, proving the existence of a family of periodic orbits. In Section 5 we define the Sun-shadow map and describe our numerical investigations.

2. Kepler's and Stark's dynamics

We consider Kepler's dynamics, defined by

$$\ddot{\boldsymbol{x}} = -\frac{\mu \boldsymbol{x}}{|\boldsymbol{x}|^3}, \tag{1}$$

with $\mu > 0$ the Earth gravitation parameter and $\boldsymbol{x} = (x, y) \in \mathbb{R}^2$. Moreover, we take into account Stark's dynamics, given by

$$\ddot{\boldsymbol{x}} = -\frac{\mu \boldsymbol{x}}{|\boldsymbol{x}|^3} + f\boldsymbol{e}_1, \tag{2}$$

where $f > 0$, $\boldsymbol{e}_1 = (1, 0)^T$. Here, T stands for vector transposition. In Eq. (2), the term $f\boldsymbol{e}_1$ models the perturbing force due to the solar radiation pressure as a constant acceleration. For Earth satellites with area-to-mass ratios between 10^{-2} m^2/kg and 10 m^2/kg, f has values between about $7 \cdot 10^{-11}$ km/s^2 and $7 \cdot 10^{-8}$ km/s^2 (see [11]).

Both Eqs. (1) and (2) can be written in Hamiltonian form, with Hamilton's functions

$$H_k = \frac{1}{2}(p_x^2 + p_y^2) - \frac{\mu}{\sqrt{x^2 + y^2}}, \tag{3}$$

$$H_s = \frac{1}{2}(p_x^2 + p_y^2) - \frac{\mu}{\sqrt{x^2 + y^2}} - fx, \tag{4}$$

where p_x, p_y are the moments conjugated to x, y. Hereafter, the labels k, s will stand for *Kepler* and *Stark*, respectively.

Besides H_k, the angular momentum

$$C_k = p_y x - p_x y \tag{5}$$

and the Laplace–Lenz vector

$$\boldsymbol{A}_k = \left(p_y(p_y x - p_x y) - \frac{\mu x}{\sqrt{x^2 + y^2}}, p_x(p_x y - p_y x) - \frac{\mu y}{\sqrt{x^2 + y^2}}\right)^T$$

are first integrals of Kepler's dynamics. Note that relation

$$|\boldsymbol{A}_k|^2 = \mu^2 + 2H_k C_k^2$$

holds among these integrals. We denote by L_k the opposite of the x-component of $\boldsymbol{A}_k$.

On the other hand, besides H_s, Stark's dynamics has the first integral

$$L_s = p_y(p_x y - p_y x) + \frac{\mu x}{\sqrt{x^2 + y^2}} - \frac{f}{2}y^2, \tag{6}$$

which is a generalisation of L_k (see [12]), but there are no other integrals independent from L_s and H_s.

2.1. Hamilton–Jacobi equations and separation of variables

Hamilton–Jacobi theory [13] is the natural tool to study Stark's problem. Indeed, the coordinate change $(x, y) \mapsto (u, v)$ defined by

$$x = \frac{u^2 - v^2}{2}, \qquad y = uv \tag{7}$$

separates the variables in the Hamilton–Jacobi equations of both Kepler's and Stark's problems. Relations (7) can be completed to a canonical transformation leading to new variables (p_u, p_v, u, v):

$$\begin{aligned} &u = \pm\sqrt{x + \sqrt{x^2 + y^2}}, \qquad v = y/u, \\ &p_u = up_x + vp_y, \qquad p_v = -vp_x + up_y. \end{aligned} \tag{8}$$

Also a transformation of the time variable t can be performed by introducing the *fictitious time* τ through the differential relation

$$\frac{d\tau}{dt} = \frac{1}{u^2 + v^2}.$$

Hereafter, we shall denote with a *prime* the derivative with respect to τ. Hamilton's functions for the two dynamics in these coordinates are

$$\mathscr{H}_k = \frac{p_u^2 + p_v^2}{2(u^2 + v^2)} - \frac{2\mu}{u^2 + v^2}, \tag{9}$$

$$\mathscr{H}_s = \frac{p_u^2 + p_v^2}{2(u^2 + v^2)} - \frac{2\mu}{u^2 + v^2} - \frac{f}{2}(u^2 - v^2). \tag{10}$$

Note that the variables introduced are similar to the ones of the Levi-Civita regularisation [14]. Indeed, setting $\boldsymbol{U} = (p_u, p_v, u, v)^T$, Stark's and Kepler's dynamical systems can be written as

$$\boldsymbol{U}' = \boldsymbol{X}_k(\boldsymbol{U}) = (2h_k u, 2h_k v, p_u, p_v)^T, \tag{11}$$

$$\boldsymbol{U}' = \boldsymbol{X}_s(\boldsymbol{U}) = \left(2h_s u + 2fu^3, 2h_s v - 2fv^3, p_u, p_v\right)^T, \tag{12}$$

where h_k and h_s are the values of $\mathscr{H}_k$ and $\mathscr{H}_s$ for some given initial conditions. Thus, the equations of motion are not singular at the origin $(u, v) = (0, 0)$, as opposite to Eqs. (1) and (2).

The angular momentum in the new coordinates is

$$\mathscr{C}_k = \frac{1}{2}(p_v u - p_u v),$$

while the integrals L_k, L_s become

$$\mathscr{L}_k = \frac{p_u^2 v^2 - p_v^2 u^2}{2(u^2 + v^2)} + \mu\frac{u^2 - v^2}{u^2 + v^2}, \tag{13}$$

$$\mathscr{L}_s = \frac{p_u^2 v^2 - p_v^2 u^2}{2(u^2 + v^2)} + \mu\frac{u^2 - v^2}{u^2 + v^2} - \frac{f}{2}u^2 v^2. \tag{14}$$

Hamilton–Jacobi equations for the two problems are

$$\left(\frac{\partial W_k}{\partial u}\right)^2 + \left(\frac{\partial W_k}{\partial v}\right)^2 = 2\big(h_k(u^2 + v^2) + 2\mu\big), \tag{15}$$

$$\left(\frac{\partial W_s}{\partial u}\right)^2 + \left(\frac{\partial W_s}{\partial v}\right)^2 = 2\big(h_s(u^2 + v^2) + 2\mu\big) + f(u^4 - v^4), \tag{16}$$

where W_k, W_s are the unknown generating functions. In (15) the variables are separated, so that we obtain

$$\begin{cases} p_u^2 - 2(h_k u^2 + \mu) = \alpha_k, \\ p_v^2 - 2(h_k v^2 + \mu) = -\alpha_k, \end{cases} \tag{17}$$

where α_k is an integration constant. Let ℓ_k be the value of the integral $\mathscr{L}_k$. Substituting p_u^2, p_v^2 given by (17) into $\mathscr{L}_k(p_u, p_v, u, v) = \ell_k$ and simplifying we get

$$\alpha_k = 2\ell_k.$$

In a similar way, from Eq. (16) we get

$$\begin{cases} p_u^2 - \left(2(h_s u^2 + \mu) + f u^4\right) = \alpha_s, \\ p_v^2 - \left(2(h_s v^2 + \mu) - f v^4\right) = -\alpha_s, \end{cases} \tag{18}$$

with

$$\alpha_s = 2\ell_s,$$

where ℓ_s is the value of the integral $\mathscr{L}_s$.

3. Trajectories in Stark's dynamics

As explained in [10], all the possible trajectories of Stark's dynamics can be divided into four categories, depending on the values ℓ_s, h_s of $\mathscr{L}_s$, $\mathscr{H}_s$.

Relations

$$p_u = \frac{du}{d\tau}, \qquad p_v = \frac{dv}{d\tau} \tag{19}$$

yield

$$\tau + A_1 = \int \frac{du}{\sqrt{U(u)}}, \tag{20}$$

$$\tau + A_2 = \int \frac{dv}{\sqrt{V(v)}}, \tag{21}$$

where A_1 and A_2 are integration constants and

$$U(u) = f u^4 + 2h_s u^2 + 2(\mu + \ell_s), \tag{22}$$

$$V(v) = -f v^4 + 2h_s v^2 + 2(\mu - \ell_s) \tag{23}$$

correspond to the expressions of p_u^2, p_v^2 in (18).

Conditions

$$U(u) \geq 0, \qquad V(v) \geq 0$$

restrict the possible configurations on the basis of the values ℓ_s, h_s. Let us set

$$\xi = u^2, \qquad \eta = v^2.$$

The polynomials $U(u)$ and $V(v)$ can be written as

$$U(u) = f(u^2 - \xi_1)(u^2 - \xi_2), \qquad V(v) = -f(v^2 - \eta_1)(v^2 - \eta_2),$$

where

$$\begin{aligned} \xi_1 &= -\frac{h_s}{f} + \sqrt{\frac{h_s^2}{f^2} - \frac{2(\mu + \ell_s)}{f}}, \\ \xi_2 &= -\frac{h_s}{f} - \sqrt{\frac{h_s^2}{f^2} - \frac{2(\mu + \ell_s)}{f}}, \\ \eta_1 &= \frac{h_s}{f} + \sqrt{\frac{h_s^2}{f^2} + \frac{2(\mu - \ell_s)}{f}}, \\ \eta_2 &= \frac{h_s}{f} - \sqrt{\frac{h_s^2}{f^2} + \frac{2(\mu - \ell_s)}{f}}, \end{aligned} \tag{24}$$

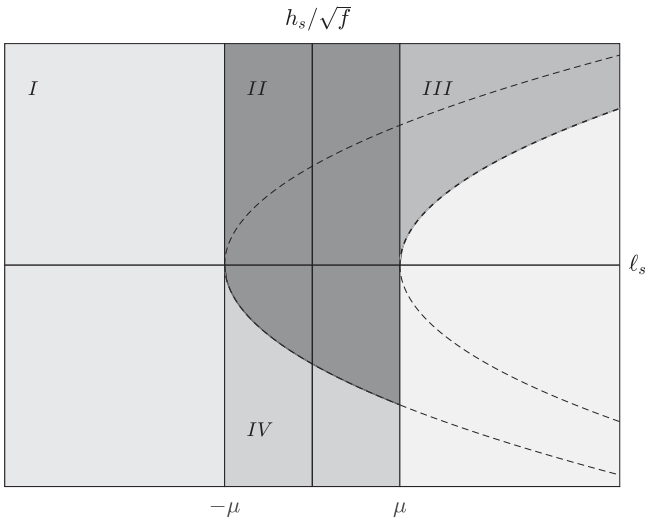

Fig. 1. Stark's problem: the four regions in the $(\ell_s, h_s/\sqrt{f})$ plane.

Table 1
Qualitative description of the trajectories in the (x, y) plane for Stark's problem. We denote by i the imaginary unit.

Region *I*	$\ell_s \in (-\infty, -\mu)$; $h_s/\sqrt{f} \in (-\infty, +\infty)$
$V(v)$, $U(u)$ roots	$v_1 > 0$, $v_2 \in i\mathbb{R}$, $u_1 > 0$, $u_2 \in i\mathbb{R}$
v, u variable	$v \in [-v_1, v_1]$, $u \in (-\infty, -u_1] \cup [u_1, +\infty)$
Trajectories type	Unbounded, self-intersecting, not encircling the origin
Region *II*	$\ell_s \in (-\mu, \mu)$; $h_s/\sqrt{f} \in (-\sqrt{2(\mu + \ell_s)}, +\infty)$
$V(v)$, $U(u)$ roots	$v_1 > 0$, $v_2 \in i\mathbb{R}$, $u_1, u_2 \in \mathbb{C} \setminus \mathbb{R}$
v, u variable	$v \in [-v_1, v_1]$, $u \in (-\infty, +\infty)$
Trajectories type	Unbounded, self-intersecting, encircling the origin
Region *III*	$\ell_s \in (\mu, +\infty)$; $h_s/\sqrt{f} \in (\sqrt{-2(\mu - \ell_s)}, +\infty)$
$V(v)$, $U(u)$ roots	$v_1 > v_2 > 0$, $u_1, u_2 \in \mathbb{C} \setminus \mathbb{R}$
v, u variable	$v \in [-v_1, -v_2] \cup [v_2, v_1]$, $u \in (-\infty, +\infty)$
Trajectories type	Unbounded, not self-intersecting
Region *IV*	$\ell_s \in (-\mu, \mu)$; $h_s/\sqrt{f} \in (-\infty, -\sqrt{2(\mu + \ell_s)})$
$V(v)$, $U(u)$ roots	$v_1 > 0$, $v_2 \in i\mathbb{R}$, $u_1 > u_2 > 0$
v, u variable	$v \in [-v_1, v_1]$, $u \in (-\infty, -u_1] \cup [-u_2, u_2] \cup [u_1, +\infty)$
Trajectories type	Two types: bounded; unbounded, self-intersecting, not encircling the origin

with $\xi_1, \xi_2, \eta_1, \eta_2 \in \mathbb{C}$. Setting

$$u_1 = \sqrt{\xi_1}, \qquad u_2 = \sqrt{\xi_2}, \qquad v_1 = \sqrt{\eta_1}, \qquad v_2 = \sqrt{\eta_2}, \tag{25}$$

the roots of $U(u)$ are $\pm u_1, \pm u_2$, and those of $V(v)$ are $\pm v_1, \pm v_2$.

It is convenient to study the problem in the $(\ell_s, h_s/\sqrt{f})$ plane. Beletsky showed that this plane can be divided into four regions as illustrated in Fig. 1. These regions do not cover completely the $(\ell_s, h_s/\sqrt{f})$ plane: in the remaining part (the brighter one in the figure) the motion is not possible. Each region is characterised by different types of trajectories listed in Table 1, see [10]. The admissible subsets of the configuration space are shown in Fig. 2: these are delimited by straight lines in the (u, v) plane, and by parabolas in the (x, y) plane. For completeness we added in Appendix Tables 2 and 3, describing the features of the trajectories at the boundaries of these regions.

Remark 1. We can have zero velocity points only for some values ℓ_s, h_s of the integrals $\mathscr{L}_s$, $\mathscr{H}_s$. For $(\ell_s, h_s/\sqrt{f})$ belonging to region *I* we have the two points

$$(x, y) \in \{(\xi_1/2 - \eta_1/2, \pm\sqrt{\xi_1\eta_1})\};$$

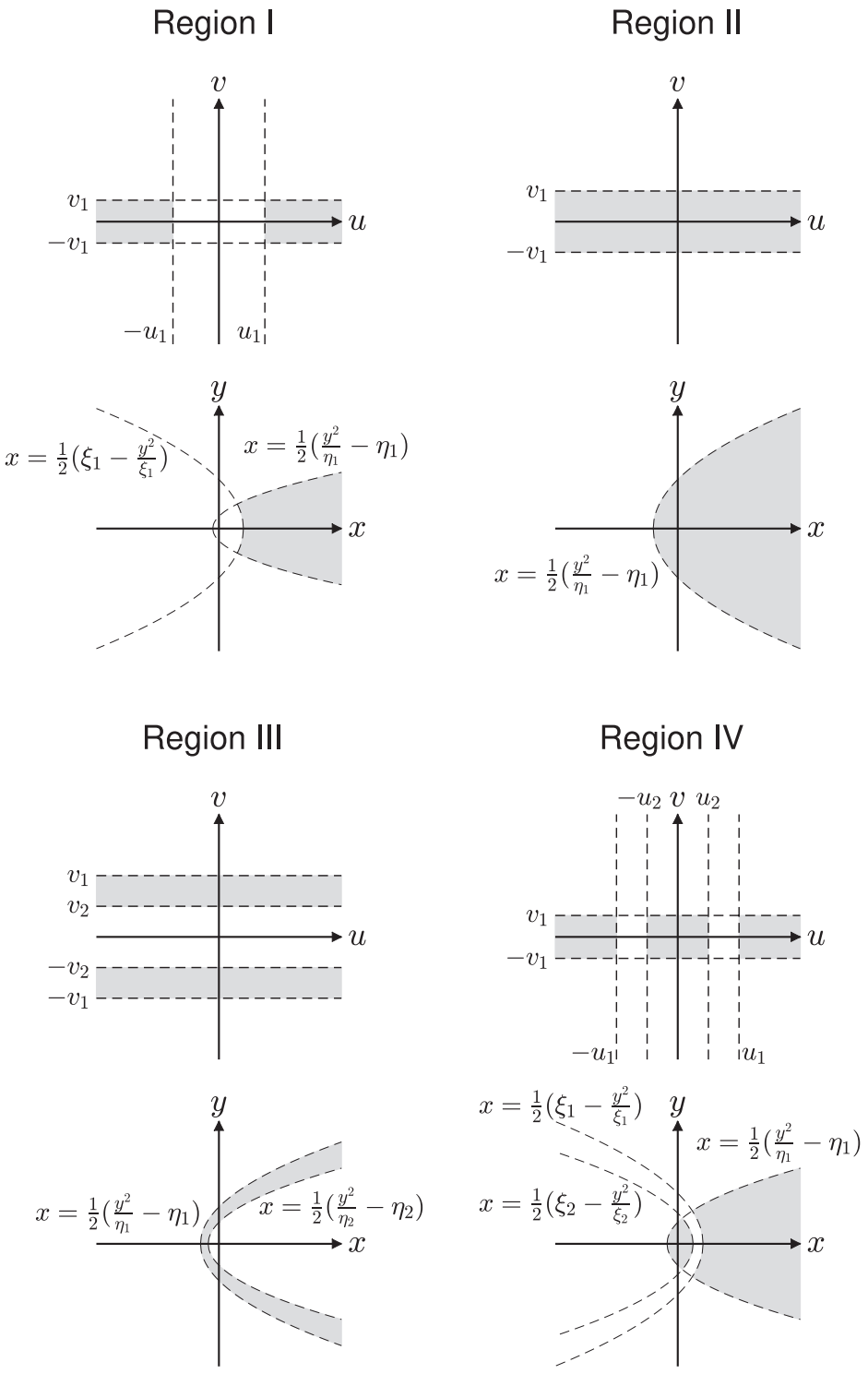

Fig. 2. Admissible subsets of the configuration space in (x, y) and (u, v) planes, depending on the region. These subsets are represented by the grey areas; the dashed lines correspond to their boundaries.

for $(\ell_s, h_s/\sqrt{f})$ in region *IV* we have the four points

$$(x, y) \in \{(\xi_1/2 - \eta_1/2, \pm\sqrt{\xi_1\eta_1}), (\xi_2/2 - \eta_1/2, \pm\sqrt{\xi_2\eta_1})\}.$$

If $(\ell_s, h_s/\sqrt{f})$ belongs to regions *II* or *III*, there cannot be zero velocity points.

Remark 2. For each region of the $(\ell_s, h_s/\sqrt{f})$ plane, the v-component of an orbit is periodic (and bounded). The u-component is periodic (and bounded) only if $(\ell_s, h_s/\sqrt{f})$ belongs to region *IV* and $u^2 \leq \xi_2$. On the contrary, the u-component is unbounded if $(\ell_s, h_s/\sqrt{f})$ belongs to one among regions *I*, *II*, *III*, or it belongs to region *IV*, and $u^2 \geq \xi_1$.

Proposition 1. *In case $u(\tau)$ and $v(\tau)$ are periodic solutions of (12), relation*

$$\frac{T_v}{T_u} < 1 \tag{26}$$

holds for their periods T_u, T_v.

Proof. The periods T_u and T_v of the u and v variables can be written as elliptic integrals:

$$T_u = \frac{4}{\sqrt{f}} \int_0^{\pi/2} \frac{d\varphi}{\sqrt{a_u^2 \cos^2\varphi + b_u^2 \sin^2\varphi}},$$

$$T_v = \frac{4}{\sqrt{f}} \int_0^{\pi/2} \frac{d\varphi}{\sqrt{a_v^2 \cos^2\varphi + b_v^2 \sin^2\varphi}},$$

where

$$a_u^2 = \xi_1 = -\frac{h_s}{f} + \sqrt{\frac{h_s^2}{f^2} - \frac{2(\mu+\ell_s)}{f}},$$

$$b_u^2 = \xi_1 - \xi_2 = 2\sqrt{\frac{h_s^2}{f^2} - \frac{2(\mu+\ell_s)}{f}},$$

$$a_v^2 = \eta_1 - \eta_2 = 2\sqrt{\frac{h_s^2}{f^2} + \frac{2(\mu-\ell_s)}{f}},$$

$$b_v^2 = -\eta_2 = -\frac{h_s}{f} + \sqrt{\frac{h_s^2}{f^2} + \frac{2(\mu-\ell_s)}{f}}.$$

Let a_u, b_u, a_v, b_v be the positive square roots of the previous quantities. We note that

$$b_u < a_u < b_v < a_v. \tag{27}$$

If $a, b \in \mathbb{R}$, with $a, b > 0$, there exists $\alpha \in \mathbb{R}^+$ such that

$$\lim_{k\to\infty} \Phi^k(a,b) = (\alpha,\alpha)$$

where $\Phi : (a,b) \mapsto \left(\frac{a+b}{2}, \sqrt{ab}\right)$. The number α is called arithmetic–geometric mean of a and b (see [15]), and we denote it by $M(a,b)$. Setting

$$I(a,b) = \int_0^{\frac{\pi}{2}} \frac{d\varphi}{\sqrt{a^2\cos^2\varphi + b^2\sin^2\varphi}},$$

if $a > b$ we have

$$I(\Phi(a,b)) = I(a,b),$$

so that we obtain

$$I(a,b) = \lim_{k\to\infty} I(\Phi^k(a,b)) = I(\alpha,\alpha) = \frac{\pi}{2\alpha} = \frac{\pi}{2M(a,b)}.$$

Thus, we get

$$T_u = \frac{2\pi}{\sqrt{f}M(a_u,b_u)}, \qquad T_v = \frac{2\pi}{\sqrt{f}M(a_v,b_v)}.$$

Since $b_u \le M(a_u,b_u) \le a_u$, and $b_v \le M(a_v,b_v) \le a_v$, from (27) we find

$$M(a_u,b_u) < M(a_v,b_v),$$

that corresponds to (26). □

3.1. Unstable periodic orbits of brake type

There exists a family of unstable periodic orbits of brake type, $\boldsymbol{x}^* = \boldsymbol{x}^*(t;\ell_s)$, parametrised by $\ell_s \in (-\mu,\mu)$. We recall that an orbit is of brake type if it passes through zero velocity points.

It is possible to analyse the behaviour of the u and v-components of the trajectory in the reduced phase spaces with coordinates (u,p_u) and (v,p_v). For this purpose, we can take into account the two Hamiltonian dynamics defined by

$$\mathsf{H}_{\mathsf{s_u}} = \frac{p_u^2}{2u^2} - \frac{2(\mu+\ell_s)+fu^4}{2u^2}, \qquad \mathsf{H}_{\mathsf{s_v}} = \frac{p_v^2}{2v^2} - \frac{2(\mu-\ell_s)-fv^4}{2v^2},$$

obtained from system (18). $\mathsf{H}_{\mathsf{s_u}}$ has the two critical points $(p_u^*, \pm u^*)$, where

$$p_u^* = 0, \qquad u^* = \left(\frac{2(\mu+\ell_s)}{f}\right)^{\frac{1}{4}}.$$

We can show that they are two unstable equilibrium points for the reduced dynamics in the (u,p_u) plane. In fact, the Jacobian of the Hamiltonian vector field $\boldsymbol{X}_{\mathsf{s_u}}$ induced by $\mathsf{H}_{\mathsf{s_u}}$, evaluated in both critical points, is

$$D\boldsymbol{X}_{\mathsf{s_u}} = \begin{bmatrix} 0 & 4f \\ \frac{1}{\xi^*} & 0 \end{bmatrix},$$

where

$$\xi^* = u^{*2}. \tag{28}$$

At these critical points, the value of $\mathsf{H}_{\mathsf{s_u}}$ is

$$h_s^* = -\sqrt{2f(\mu+\ell_s)}, \tag{29}$$

so that

$$\xi^* = -\frac{h_s^*}{f} \tag{30}$$

and $\det D\boldsymbol{X}_{\mathsf{s_u}} < 0$ at $(p_u^*, \pm u^*)$.

The level set $\mathsf{H}_{\mathsf{s_v}} = h_s^*$ (see Fig. 3) corresponds to the (v,p_v)-projection of the solution of (12), with $h_s = h_s^*$. This solution is defined also in $v = 0$ and is periodic. This implies that, if $\ell_s \in (-\mu,\mu)$ and Stark's Hamiltonian $\mathscr{H}_s$ has the value h_s^*, we have two unstable periodic orbits in the (u,v) plane. They have a constant value of the u-component, equal to $\pm u^*$, and a constant value of p_u, equal to zero. Moreover, they are of brake type because each of them develops between two zero velocity points. These are given by $(u^*, \pm v_1^*)$, with $v_1^* = v_1(h_s^*)$, in one case, and by $(-u^*, \pm v_1^*)$ in the other. In the (x,y) plane, they correspond to the same periodic orbit $\boldsymbol{x}^*$, which is a parabolic arc and develops between the zero velocity points $(\xi^*/2 - \eta_1^*/2, \pm\sqrt{\xi^*\eta_1^*})$, where $\eta_1^* = v_1^{*2}$. Its trajectory is shown in Fig. 4.

The family of brake orbits $\boldsymbol{x}^*$ exists for values ℓ_s, h_s corresponding to the boundary between regions *II* and *IV*. On this boundary, the values of ξ_1 and ξ_2 coincide and are equal to ξ^*.

Remark 3. For $h_s < h_s^*$ (region *IV*), we have $\xi_2 < \xi^* < \xi_1$.

To produce Fig. 3 as well as all the other figures in the paper, we used values of the parameters which are compatible with Stark's problem for Earth satellites.

3.2. Other periodic orbits

There exists another family of orbits of brake type parametrised by h_s at the boundary of region *I*, i.e. for $\ell_s = -\mu$. These are collision orbits, which can be prolonged to periodic orbits in the regularised variables u, v. They have a constant value of the u-coordinate, equal to zero, in the (u,v) plane, therefore they lie on the x axis in the (x,y) plane. Moreover, there are collision orbits of brake type in correspondence of $\ell_s = \mu$ and $h_s < -2\sqrt{f\mu}$ that also can be extended to periodic ones. They have a constant value of the v-coordinate, equal to zero, thus they lie on the x axis in the (x,y) plane. If $h_s = -2\sqrt{f\mu}$, we obtain the two fixed points $(u,v) = (\pm\sqrt{|h_s|/f}, 0)$ for Stark's dynamics, corresponding to a single fixed point in the (x,y) plane.

Additional periodic orbits (in the (u,v) plane) can exist for $(\ell_s, h_s/\sqrt{f})$ belonging to region *IV*, as a consequence of Remark 2. Their peculiarity is that the periods T_u and T_v are commensurable, that is their quotient T_v/T_u is rational. In Fig. 5 some examples are shown. Note that the orbits in Figs. 5(c) and 5(d) are of brake type. In this case, if $T_v/T_u = m/k$ with m and k two odd positive integers, $m < k$, the trajectory passes through the origin as shown in Fig. 5(d), where $m = 1$ and $k = 3$.

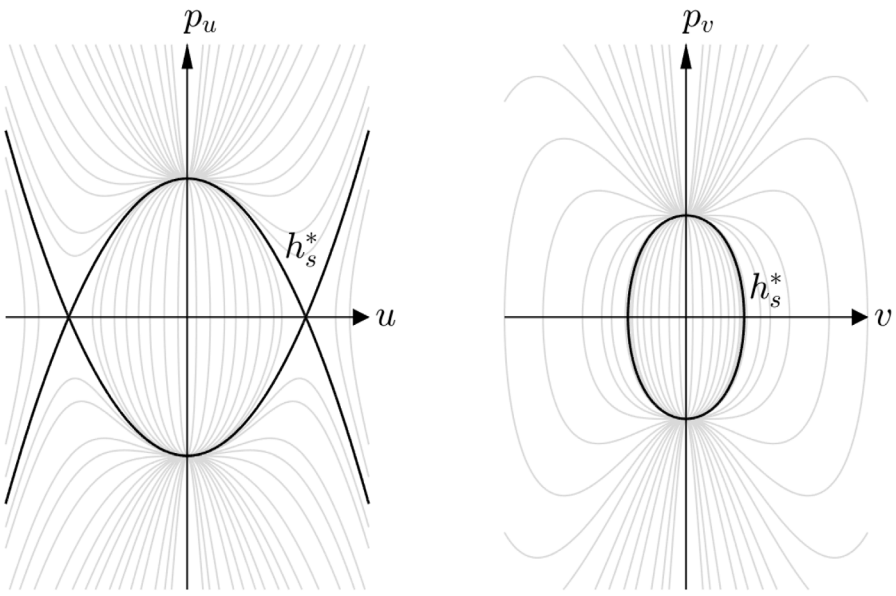

Fig. 3. Stark's problem: phase portraits in the (u, p_u) and (v, p_v) planes, for $\ell_s = 119\,580$ km^3/s^2, $f = 9.12 \times 10^{-9}$ km/s^2.

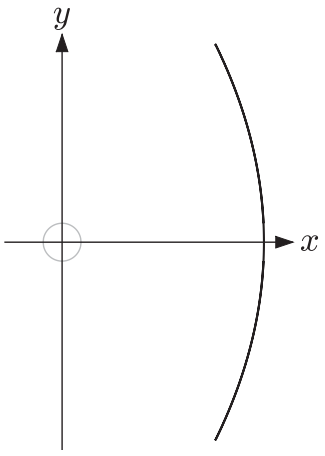

Fig. 4. Stark's problem: unstable periodic orbit of brake type.

4. The Sun-shadow dynamics

The Sun-shadow problem arises by switching dynamics each time the satellite passes through the boundary of the Earth shadow. The flow develops by alternating Kepler's regime, corresponding to the shadow region, and Stark's regime, in the out-of-shadow region. As shown in Fig. 6, the shadow region is defined as the set $\{(x, y) : \ x \geq 0, \ -R \leq y \leq R\}$ in the (x, y) plane. In the (u, v) plane this region has two components: it is the set $\{(u, v) : \ -R/|u| \leq v \leq R/|u|, \ |u| \geq \sqrt{R}\}$.

At the time $t = 0$ of entrance into the shadow, let us consider initial conditions belonging to the set

$$\left\{(p_u, p_v, u, v) : \ u > \sqrt{R}, \ uv = -R, \ p_v u + p_u v > 0\right\}. \tag{31}$$

The last condition is needed to have the velocity vector pointing inside the shadow region. We search for the solutions (p_u, p_v, u, v) of the polynomial system

$$\begin{cases} p_u^2 = 2h_k u^2 + 2(\mu + \ell_k) \\ p_v^2 = 2h_k v^2 + 2(\mu - \ell_k) \\ 2c_k = p_v u - p_u v \\ uv = R \end{cases} \tag{32}$$

with

$$u > \sqrt{R}, \qquad v > 0,$$

where c_k is the value of the angular momentum $\mathscr{C}_k$. From system (32), it is possible to obtain the state at the exit point of the shadow region. By eliminating the variables p_u, p_v, v we obtain an eight degree polynomial equation in u:

$$\begin{aligned} &(\mu - \ell_k)^2 u^8 - 4(\mu - \ell_k) c_k^2 u^6 + 2\big(R^2(\ell_k^2 - \mu^2 - 4c_k^2 h_k) + 2c_k^4\big)u^4 \\ &- 4(\mu + \ell_k) R^2 c_k^2 u^2 + 4(\mu + \ell_k)^2 R^4 = 0. \end{aligned} \tag{33}$$

The roots of (33) come in pairs $\pm u$, which give the same values of x. We can select the right value of x using the y-component of the Laplace–Lenz integral $\boldsymbol{A}_k$. Let us call $\boldsymbol{U}_i = (p_{u_i}, p_{v_i}, u_i, v_i)^T$ the selected solution, corresponding to the state at the entrance point in Stark's regime. To find the exit point from this regime $\boldsymbol{U}_o = (p_{u_o}, p_{v_o}, u_o, v_o)^T$, we match the time intervals of u and v to go from $\boldsymbol{U}_i$ to $\boldsymbol{U}_o$, which can be computed from Eqs. (20), (21).

In Stark's regime, the angular momentum can change not only in value, but even in sign. Indeed, the satellite can re-enter Kepler's regime either in the first or third quadrant of the (u, v) plane.

Proposition 2. *Each time the satellite crosses the boundary of the shadow region, we have a leap in energy from h_s to h_k, or vice versa: the variation is equal to $\pm f(\bar{u}^2 - R^2/\bar{u}^2)/2$, where $\bar{u}$ is the value taken by u at the crossing point. A similar leap occurs from ℓ_s to ℓ_k, or vice versa. In this case, the variation is equal to $\pm fR^2/2$. When the satellite goes back to Stark's regime, the value of $\mathscr{L}_s$ is the same as before crossing the shadow; on the other hand, the energy usually changes unless the orbit is symmetric with respect to the u axis.*

Proof. Assume that the body enters Stark's regime at the point $(p_{u_{i,1}}, p_{v_{i,1}}, u_{i,1}, v_{i,1})$. Let $h_s^{i,1}$ be the value of the energy and $\ell_s^{\,i,1}$ the value of the Laplace–Lenz integral. When the body returns to the shadow region, the integrals vary in the following way:

$$h_k^{o,1} = h_s^{i,1} + \frac{f}{2}\left(u_{o,1}^2 - \frac{R^2}{u_{o,1}^2}\right),$$

$$\ell_k^{\,o,1} = \ell_s^{\,i,1} + \frac{f}{2}R^2,$$

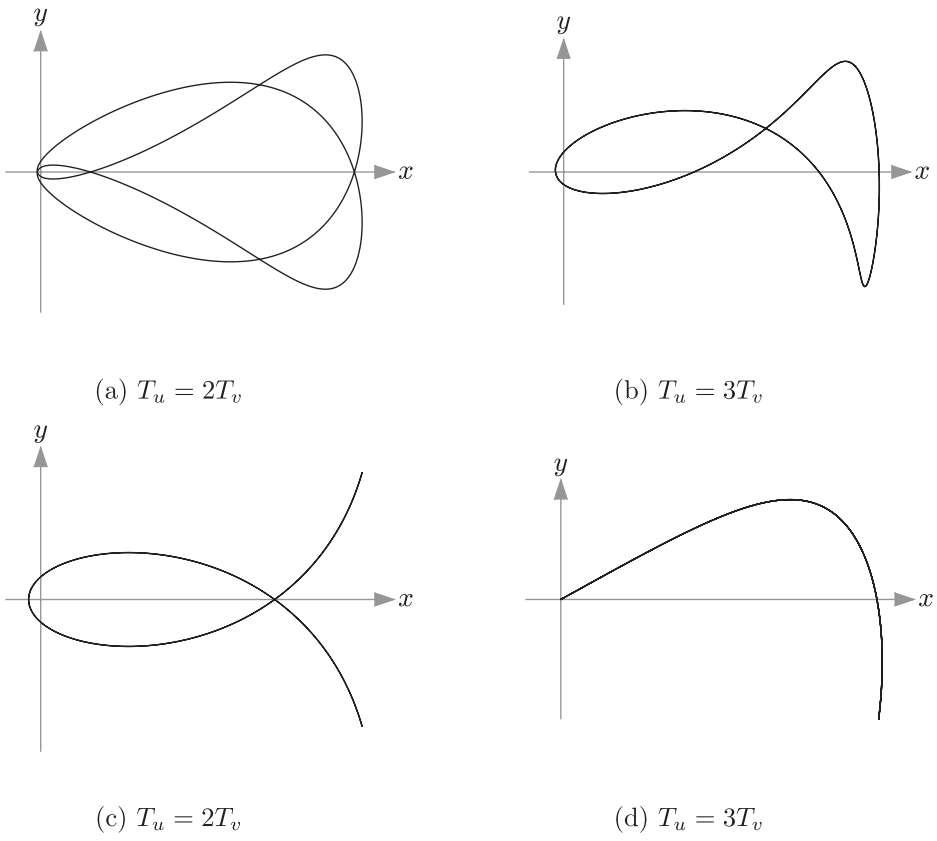

Fig. 5. Stark's problem: some periodic orbits, with $\ell_s = 348\,600$ km^3/s^2, $f = 9.12 \times 10^{-9}$ km/s^2.

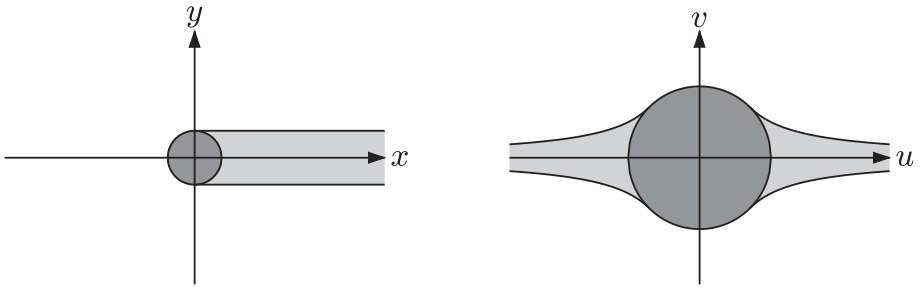

Fig. 6. Sun-shadow regions in the (x, y) plane (left), (u, v) plane (right).

with $u_{o,1}$ denoting the u coordinate of the point on the shadow boundary where the satellite exits from Stark's regime. When the body enters Stark's regime again, by passing through the point $(p_{u_{i,2}}, p_{v_{i,2}}, u_{i,2}, v_{i,2})$, similar variations occur:

$$h_s^{i,2} = h_k^{o,1} - \frac{f}{2}\left(u_{i,2}^2 - \frac{R^2}{u_{i,2}^2}\right),$$

$$\ell_s^{\,i,2} = \ell_k^{\,o,1} - \frac{f}{2}R^2.$$

Thus, we get

$$h_s^{i,2} = h_s^{i,1} + \frac{f}{2}\left(1 + \frac{R^2}{u_{o,1}^2 u_{i,2}^2}\right)\left(u_{o,1}^2 - u_{i,2}^2\right),$$

$$\ell_s^{\,i,2} = \ell_s^{\,i,1},$$

where $h_s^{i,2} = h_s^{i,1}$ only if $u_{o,1} = u_{i,2}$. □

4.1. Periodic orbits of brake type

We prove the existence of a family of periodic orbits of brake type, $\widehat{\boldsymbol{x}} = \widehat{\boldsymbol{x}}(t; \ell_s)$, parametrised by ℓ_s, which are close to the brake periodic orbits $\boldsymbol{x}^* = \boldsymbol{x}^*(t; \ell_s)$ of Stark's problem, described in Section 3.1. For this purpose, we consider values ℓ_s in $(-\mu, \mu)$, for which the periodic orbits $\boldsymbol{x}^*$ exist. In the following we shall restrict the interval $(-\mu, \mu)$ for technical reasons, related to the proof.

The idea of the proof is to search for an initial point $(x, y) = (x_0, 0)$ with $x_0 > R$, i.e. in Kepler's regime, allowing to arrive at a zero velocity point (x_B, y_B) in Stark's regime after passing through an exit point (x_E, R) from the shadow region. We look for an orbit that is symmetric with respect to the x axis, like $\boldsymbol{x}^*$. Because of the symmetry, $\widehat{\boldsymbol{x}}$ oscillates between the points (x_B, y_B) and $(x_B, -y_B)$. We search for an initial value x_0 fulfilling

$$x_0 > \xi^*/2, \tag{34}$$

where $(\xi^*/2, 0)$ belongs to $\boldsymbol{x}^*$, see Fig. 7(a). The idea behind this choice is that, passing through the shadow, the pushing effect of

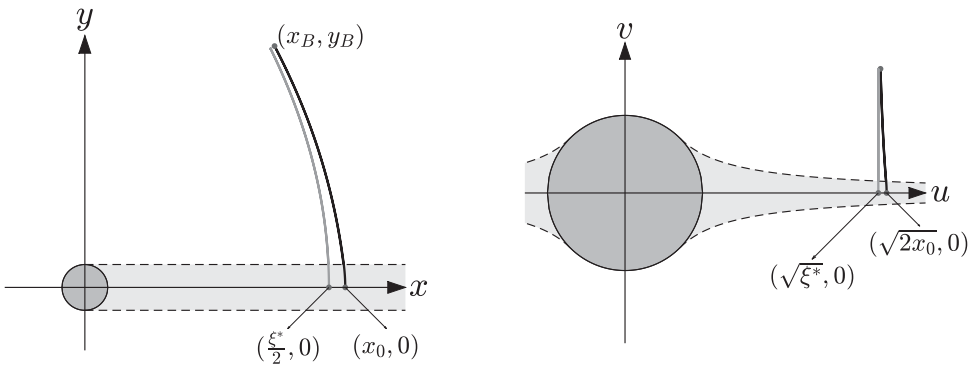

(a) (x, y) plane (b) (u, v) plane

Fig. 7. A portion of the brake orbit $\widehat{\boldsymbol{x}}(t; \ell_s)$ between the horizontal axis and a zero velocity point is represented by the black curve in the (x, y) and (u, v) coordinates. The analogous portion of the brake orbit $\boldsymbol{x}^*(t; \ell_s)$ of Stark's problem is drawn in grey.

the solar radiation pressure is lacking. Moreover, we require that x_0 is such that at the exit point (x_E, R) the energy h_s fulfils

$$h_s < h_s^*, \tag{35}$$

with h_s^* given in (29). If $h_s > h_s^*$ we cannot have zero velocity points, see Remark 1.

For the proof, we use the variables u, v. The initial point $(x_0, 0)$ corresponds to two possible points $(\pm\sqrt{2x_0}, 0)$ in the (u, v) plane. Similarly, the point $(\xi^*/2, 0)$ corresponds to $(\pm\sqrt{\xi^*}, 0)$. By symmetry, we can focus only on the $\{u > 0\}$ half-plane of the (u, v) plane, see Fig. 7(b).

Proposition 3. *Let*

$$\xi_E = x_0 + x_T, \tag{36}$$

with

$$x_T = \sqrt{x_0^2 - a_k R^2}, \qquad a_k = \frac{\mu + \ell_k}{\mu - \ell_k}, \tag{37}$$

and

$$\ell_k = \ell_s + \frac{f}{2}R^2. \tag{38}$$

If x_0 is selected so that relations (34), (35) hold, then the exit point (x_E, R) from the shadow region, with

$$x_E = \frac{\xi_E}{2} - \frac{R^2}{2\xi_E}, \tag{39}$$

belongs to the unbounded component of the configuration set corresponding to region IV of Stark's regime.

Proof. Because of the symmetry of the orbit with respect to the x axis, in Kepler's regime the initial state has the form

$$(p_u, p_v, u, v) = (0, p_{v_0}, \sqrt{2x_0}, 0).$$

By system (32) we have

$$p_{v_0} = \sqrt{2(\mu - \ell_k)} \tag{40}$$

and

$$h_k = -\frac{\mu + \ell_k}{2x_0},$$

with ℓ_k defined in (38). Note from relations (40), (38) that we need to restrict the interval of ℓ_s to $(-\mu, \mu - \frac{f}{2}R^2)$.

The exit point from the shadow is obtained by solving

$$\begin{cases} p_u^2 = 2h_k u^2 + 2(\mu + \ell_k) \\ p_v^2 = 2h_k v^2 + 2(\mu - \ell_k) \\ uv = R \\ p_u p_v = 2uvh_k, \end{cases} \tag{41}$$

where $p_v > 0$. With the last equation we set to zero the y-component of the Laplace–Lenz vector, which is a necessary condition for the symmetry with respect to the x axis. There are four possible real solutions of (41), and two of them have positive values of u. Between these two, only one corresponds to exiting from the shadow, i.e. fulfils

$$p_y = \frac{up_v + vp_u}{u^2 + v^2} > 0.$$

This solution gives the u coordinate at the exit point, whose square is ξ_E, given by (36). From ξ_E, we obtain x_E through relation (39), applying the coordinates change (7). Using relation (34), we can write

$$x_0 = \xi^*/2 + \Delta x.$$

We have real values of ξ_E if and only if

$$\Delta x \in \left(-\infty, -\frac{\xi^*}{2} - \sqrt{a_k}R\right] \cup \left[-\frac{\xi^*}{2} + \sqrt{a_k}R, +\infty\right).$$

The last condition is fulfilled for each choice of $\Delta x \geq 0$ if

$$-\frac{\xi^*}{2} + \sqrt{a_k}R \leq 0, \tag{42}$$

which holds if we further restrict the interval of ℓ_s to $[\ell_s^-, \ell_s^+]$, with

$$\ell_s^{\pm} = -\frac{5}{4}fR^2 \pm \sqrt{\mu^2 + \frac{9}{16}f^2R^4 - \frac{5}{2}fR^2\mu}.$$

Remark 4. Since $f \ll 1$, the new range $[\ell_s^-, \ell_s^+]$ is slightly smaller than $(-\mu, \mu - \frac{f}{2}R^2)$.

The energy in Stark's regime is

$$\mathsf{h}_s(x_0) = -\frac{\mu + \ell_k}{2x_0} - \frac{f}{2}(x_0 + x_T) + \frac{fR^2}{2(x_0 + x_T)}. \tag{43}$$

For the proof we need this result:

Lemma 1. *The energy* h_s *is a decreasing function of* x_0 *in the interval* $[\frac{\xi^*}{2}, +\infty)$*. Moreover, we have*

$\mathsf{h}_s(\xi^*/2) > h_s^*$.

Proof. From Eq. (43), the derivative of h_s with respect to x_0 is

$$\frac{d\mathsf{h}_s}{dx_0} = \frac{(\mu+\ell_k)(x_0+x_T)x_T - f(x_0+x_T)^2x_0^2 - fR^2x_0^2}{2(x_0+x_T)x_0^2x_T}.$$

The denominator is always positive, being $x_0, x_T > 0$. We prove that the numerator is negative. Because of relations (29), (30) and (38), this corresponds to showing that

$$(x_0+x_T)\left(\frac{\xi^{*2}}{2}x_T - (x_0+x_T)x_0^2\right) + R^2\left(\frac{1}{2}(x_0+x_T)x_T - x_0^2\right) < 0.$$

This follows from (34) and $x_0 > x_T$. We conclude that $\frac{d\mathsf{h}_s}{dx_0} < 0$.

Next we prove the second statement of the lemma. We have

$$\mathsf{h}_s\left(\frac{\xi^*}{2}\right) - h_s^* = -\frac{\mu+\ell_k}{\xi^*} - \frac{f}{4}\left(\xi^* + \sqrt{\xi^{*2} - 4a_kR^2}\right) + \frac{fR^2}{\xi^* + \sqrt{\xi^{*2} - 4a_kR^2}} - h_s^*.$$

Using (29), (30), (38) we obtain

$$-\frac{\mu+\ell_k}{\xi^*} = \frac{h_s^*}{2} + \frac{f^2R^2}{2h_s^*}$$

and we get

$$\mathsf{h}_s\left(\frac{\xi^*}{2}\right) - h_s^* = \left(h_s^* + \sqrt{h_s^{*2} - 4a_kf^2R^2}\right) \times \left(-\frac{1}{4} + \frac{f^2R^2}{2h_s^*\left(-h_s^* + \sqrt{h_s^{*2} - 4a_kf^2R^2}\right)}\right).$$

From relation

$$h_s^* + \sqrt{h_s^{*2} - 4a_kf^2R^2} < 0,$$

we conclude that $\mathsf{h}_s(\xi^*/2) - h_s^* > 0$. □

Using Lemma 1, we only need to find $x_0^* > \xi^*/2$ such that $\mathsf{h}_s(x_0^*) = h_s^*$ to prove that at the exit time the values of the integrals $(\ell_s, \mathsf{h}_s(x_0))$, with $x_0 > x_0^*$, belong to region IV. From (29), (30), (37), (38), and (43), solving equation $\mathsf{h}_s(x_0) = h_s^*$ corresponds to searching for the roots of

$$g(x_0) = -4x_0^3 + 4\xi^*x_0^2 + \left(R^2 - \xi^{*2} + 2a_kR^2\right)x_0 - \left((2x_0 - \xi^*)^2 + R^2\right)x_T.$$

From relations (34) and (37), it holds

$$Cx_0 < x_T < x_0, \qquad C = \sqrt{1 - 4a_k\frac{R^2}{\xi^{*2}}}. \tag{44}$$

Thus, we have

$$g_-(x_0) \le g(x_0) \le g_+(x_0),$$

where

$$g_-(x_0) = -2x_0\left(4x_0^2 - 4\xi^*x_0 + \xi^{*2} - a_kR^2\right),$$

$$g_+(x_0) = -(1+C)x_0 \times \left(4x_0^2 - 4\xi^*x_0 + \xi^{*2} - \frac{1-C}{1+C}R^2 - \frac{2}{1+C}a_kR^2\right).$$

The polynomials g_+ and g_- have three roots, but only one is larger than $\xi^*/2$. Denoting the latter with x_0^+ and x_0^-, respectively, we get

$$x_0^- = \frac{\xi^*}{2} + C_1, \qquad x_0^+ = \frac{\xi^* + C_2}{2},$$

with

$$C_1 = \frac{R}{2}\sqrt{a_k}, \qquad C_2 = R\sqrt{\frac{1 - C + 2a_k}{1+C}}.$$

This shows the existence of $x_0^* > \xi^*/2$, solution of $\mathsf{h}_s(x_0) = h_s^*$.

Next we show that the exit point belongs to the unbounded component of the configuration set, i.e. that $\xi_E > \xi_1$ holds for each $x_0 > x_0^*$. Since $x_0^- < x_0^* < x_0^+$ and ξ_E, given in (36), is an increasing function of x_0, we have

$$\xi_E(x_0^-) < \xi_E(x_0^*) < \xi_E(x_0^+), \tag{45}$$

where

$$\xi_E(x_0^-) = \frac{\xi^*}{2} + C_1 + \sqrt{\left(\frac{\xi^*}{2} + C_1\right)^2 - a_kR^2},$$

$$\xi_E(x_0^+) = \frac{\xi^* + C_2}{2} + \sqrt{\frac{(\xi^* + C_2)^2}{4} - a_kR^2}.$$

Relation (42) implies $\xi_E(x_0^-) > \xi^*$. Thus $\xi_E(x_0^*) > \xi^*$. Since in region IV we have $\xi_2 < \xi^* < \xi_1$, and $\xi_E < \xi_2$ or $\xi_E > \xi_1$, the latter relation holds. This concludes the proof of Proposition 3. □

Remark 5. Proposition 3 yields

$$2x_0 > \xi_E > \xi_1 > \xi^* > \xi_2 > 0,$$

and

$$\xi^* + C_1 < \xi_E^* < \xi^* + C_2,$$

where $\xi_E^* = \xi_E(x_0^*)$.

To search for a zero velocity point (x_B, y_B) we use the coordinates u, v and the fictitious time τ. The maps $u(\tau)$, $v(\tau)$ become stationary at $\tau = \tau_u, \tau_v$, respectively, where

$$\tau_u = \int_{u_1}^{\sqrt{\xi_E}} \frac{du}{\sqrt{fu^4 + 2h_su^2 + 2(\mu+\ell_s)}},$$

$$\tau_v = \int_{\frac{R}{\sqrt{\xi_E}}}^{v_1} \frac{dv}{\sqrt{-fv^4 + 2h_sv^2 + 2(\mu-\ell_s)}}.$$

We search for a value of x_0 such that

$$\tau_u = \tau_v, \tag{46}$$

which corresponds to reach a zero velocity point, see Fig. 8.

From now on, we use $h_s \in J = (-\infty, h_s^*)$ as independent variable, in place of x_0. Following [10] we can write the integrals τ_u, τ_v as

$$\tau_u(h_s) = \frac{1}{\sqrt{f\xi_1}}\int_0^{\arcsin r_\xi} \frac{d\varphi}{\sqrt{1 - \frac{\xi_2}{\xi_1}\sin^2\varphi}}, \tag{47}$$

$$\tau_v(h_s) = \frac{1}{\sqrt{f\Delta\eta}}\int_0^{\arcsin\sqrt{1-\frac{R^2}{\xi_E\eta_1}}} \frac{d\varphi}{\sqrt{1 - \frac{\eta_1}{\Delta\eta}\sin^2\varphi}}, \tag{48}$$

where

$$r_\xi = \sqrt{\frac{\xi_E - \xi_1}{\xi_E - \xi_2}}, \qquad \Delta\eta = \eta_1 - \eta_2.$$

We use the result proved below.

Lemma 2. *The following properties hold:*

(i) τ_u *is a strictly increasing function of* h_s *and*

$$\lim_{h_s \to h_s^*} \tau_u = +\infty, \tag{49}$$

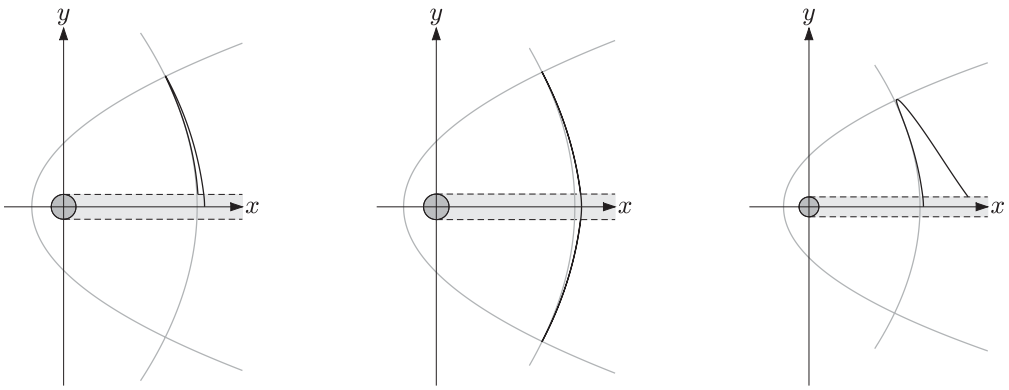

(a) $\tau_u < \tau_v$ (b) $\tau_u = \tau_v$ (c) $\tau_u > \tau_v$

Fig. 8. Brake orbit (b) and two close trajectories (a) and (c). The grey arcs of parabola represent the boundaries defining the unbounded admissible subset of the configuration space in Stark's regime (see Fig. 2 for a comparison).

(ii) τ_v fulfils

$$\limsup_{h_s \to h_s^*} \tau_v < +\infty. \tag{50}$$

Proof. (i) The derivative of τ_u with respect to h_s can be written as

$$\frac{d\tau_u}{dh_s} = \frac{1}{\sqrt{f\xi_1}} \frac{1}{\Delta\xi} \times \left(\frac{1}{f} \int_0^{\arcsin r_\xi} \frac{1 + \frac{\xi_2}{\xi_1} \sin^2\varphi}{\left(1 - \frac{\xi_2}{\xi_1} \sin^2\varphi\right)^{\frac{3}{2}}} d\varphi + \frac{1}{2} \sqrt{\frac{\xi_1}{\xi_E}} \frac{\xi_E - \xi_2}{r_\xi} \frac{dr_\xi^2}{dh_s} \right),$$

where

$$\Delta\xi = \xi_1 - \xi_2.$$

Therefore, to prove that τ_u is strictly increasing, it is sufficient to show that

$$\frac{dr_\xi^2}{dh_s} = \frac{d}{dh_s}\left(\frac{\xi_E - \xi_1}{\xi_E - \xi_2}\right) > 0. \tag{51}$$

From relations

$$\frac{d\xi_1}{dh_s} = -\frac{2\xi_1}{f\Delta\xi} < 0, \qquad \frac{d\xi_2}{dh_s} = \frac{2\xi_2}{f\Delta\xi} > 0,$$
$$\frac{d\xi_E}{dh_s} = \frac{\xi_E}{\frac{(\mu+\ell_k)x_T}{2x_0^2} - \frac{f}{2}\xi_E - \frac{f}{2}\frac{R^2}{\xi_E}} < 0,$$

where the latter follows from (30), (36), (38) and $x_0 > x_T$, we see that

$$\frac{d(\xi_E - \xi_2)}{dh_s} < 0.$$

Moreover, we have

$$\frac{d(\xi_E - \xi_1)}{dh_s} > 0, \tag{52}$$

in fact, relations (30), (36) and (38) yield that (52) is equivalent to

$$R^2\xi_1\left(\frac{1}{x_0 + x_T} - \frac{x_T}{2x_0^2}\right) + \xi_E\xi_2 - \xi_1\frac{\xi^{*2}}{2x_0^2}x_T > 0,$$

which follows from $x_0 > x_T$, $\xi_2 = \xi^{*2}/\xi_1$ (see (24) and (30)), and Remark 5. This proves (51).

Furthermore, we have

$$\lim_{h_s \to h_s^*} \xi_1 = \lim_{h_s \to h_s^*} \xi_2 = \xi^*,$$

so that

$$\lim_{h_s \to h_s^*} \tau_u = \frac{1}{\sqrt{f\xi^*}} \int_0^{\frac{\pi}{2}} \frac{d\varphi}{\sqrt{1 - \sin^2\varphi}} = +\infty.$$

This concludes the proof of (i).

(ii) We have

$$\tau_v < \frac{1}{\sqrt{f\Delta\eta}} \int_0^{\pi/2} \frac{d\varphi}{\sqrt{1 - \frac{\eta_1}{\Delta\eta}\sin^2\varphi}} = \frac{1}{\sqrt{f\Delta\eta}} \frac{\pi}{2M\left(1, \sqrt{1 - \frac{\eta_1}{\Delta\eta}}\right)},$$

where $M(a, b)$ is the arithmetic–geometric mean of a and b (see Section 3), so that

$$\limsup_{h_s \to h_s^*} \tau_v \le \frac{\pi}{2\sqrt[4]{\mu f}} \frac{1}{2\sqrt{1 - \frac{-\xi^* + 2\sqrt{\mu f}}{4\sqrt{\mu f}}}} < +\infty. \quad \square$$

Using the previous result, to show that a solution of (46) exists, we only need to find a value $\bar{h}_s$ of the energy $h_s \in J$ such that

$$\tau_v(\bar{h}_s) > \tau_u(\bar{h}_s).$$

For this purpose, we prove the following:

Lemma 3. *There exist $\bar{h}_s \in J$ and two continuous functions $\tilde{\tau}_u(h_s)$, $\tilde{\tau}_v(h_s)$ such that*

$$\tau_v(h_s) > \tilde{\tau}_v(h_s), \quad \tilde{\tau}_u(h_s) > \tau_u(h_s), \quad \forall h_s \in J$$

and

$$\tilde{\tau}_v(\bar{h}_s) = \tilde{\tau}_u(\bar{h}_s).$$

Proof. Using relation

$$\sqrt{1 - \frac{\eta_1}{\Delta\eta}\sin^2\varphi} < 1$$

we get

$$\tau_v > \frac{1}{\sqrt{f\Delta\eta}} \arcsin\sqrt{1 - \frac{R^2}{\xi_E\eta_1}}$$

in the interval J, where the function $\xi_E\eta_1$ is decreasing. Indeed, we have

$$\frac{d(\xi_E\eta_1)}{dh_s} = \frac{\xi_E\eta_1}{f}\left(\frac{1}{\sqrt{\frac{h_s^2}{f^2}+\frac{2(\mu-\ell_s)}{f}}} - \frac{1}{\frac{\xi_E}{2}+\frac{R^2}{2\xi_E}-\frac{(\mu+\ell_k)x_T}{2fx_0^2}}\right) < 0$$

which follows from (43), $x_0 > x_T$ and $\ell_s \in [\ell_s^-, \ell_s^+]$. Thus

$$\xi_E\eta_1 > \xi_E^*\eta_1^*, \qquad \eta_1^* = \eta_1(h_s^*) = -\xi^* + 2\sqrt{\mu/f}.$$

Since $\xi_E^* > \xi^*$ (see Remark 5), we obtain

$$\frac{1}{\sqrt{f\,\Delta\eta}}\arcsin\sqrt{1-\frac{R^2}{\xi_E\eta_1}} > \frac{1}{\sqrt{f\,\Delta\eta}}\arcsin\sqrt{1-\frac{R^2}{\xi^*\eta_1^*}}.$$

Moreover, we have

$$\left(\frac{\Delta\eta}{2}\right)^{\frac{1}{2}} = \left(\frac{h_s^2}{f^2}+\frac{2(\mu-\ell_s)}{f}\right)^{1/4} < \left(\xi_1^2+\frac{2(\mu-\ell_s)}{f}\right)^{1/4} < \left(\xi_1+\sqrt{\frac{2(\mu-\ell_s)}{f}}\right)^{1/2}.$$

Hence, we can set

$$\tilde\tau_v(h_s) = \frac{1}{\sqrt{2f}\left(\xi_1+\sqrt{\frac{2(\mu-\ell_s)}{f}}\right)^{1/2}}\arcsin\sqrt{1-\frac{R^2}{\xi^*\eta_1^*}}$$

so that

$$\tau_v(h_s) > \tilde\tau_v(h_s).$$

Then, using

$$\sqrt{1-\frac{\xi_2}{\xi_1}\sin^2\varphi} > \cos\varphi,$$

we get

$$\tau_u < \frac{1}{2}\frac{1}{\sqrt{f\xi_1}}\log\left(1+\frac{2r_\xi}{1-r_\xi}\right) < \frac{1}{\sqrt{f\xi_1}}\left(\frac{r_\xi}{1-r_\xi}\right)$$
$$= \frac{1}{\sqrt{f\xi_1}}\left(\frac{1}{\sqrt{1+\frac{\Delta\xi}{\xi_E-\xi_1}}-1}\right) < \frac{1}{\sqrt{f\xi_1}}\left(\frac{1}{\sqrt{1+\frac{\Delta\xi}{C_2}}-1}\right)$$

which follows from $0 < r_\xi < 1$ for $h_s \in J$, (52) and Remark 5. Using relation

$$\left(1+\frac{1}{\xi_1}\sqrt{\frac{2(\mu-\ell_s)}{f}}\right)^{1/2} < \left(1+\frac{1}{\xi^*}\sqrt{\frac{2(\mu-\ell_s)}{f}}\right)^{1/2}$$

we can set

$$\tilde\tau_u(h_s) = \frac{1}{\sqrt{f}}\frac{\left(1+\frac{1}{\xi^*}\sqrt{\frac{2(\mu-\ell_s)}{f}}\right)^{1/2}}{\left(\xi_1+\sqrt{\frac{2(\mu-\ell_s)}{f}}\right)^{1/2}}\frac{1}{\sqrt{1+\frac{\Delta\xi}{C_2}}-1},$$

so that

$$\tau_u(h_s) < \tilde\tau_u(h_s).$$

Let us introduce

$$K_1 = \sqrt{2}\left(1+\frac{1}{\xi^*}\sqrt{\frac{2(\mu-\ell_s)}{f}}\right)^{1/2}, \qquad K_2 = \arcsin\sqrt{1-\frac{R^2}{\xi^*\eta_1^*}}.$$

We obtain $\tilde\tau_u(\bar h_s) = \tilde\tau_v(\bar h_s)$ for

$$\bar h_s = -f\left(\xi^{*2}+\frac{C_2^2}{4}\frac{K_1^2}{K_2^2}\left(2+\frac{K_1}{K_2}\right)^2\right)^{1/2}. \quad \square \tag{53}$$

This concludes the proof of the existence of a family of brake periodic orbits $\widehat{\boldsymbol{x}}(t;\ell_s)$ parametrised by ℓ_s.

5. The Sun-shadow map

To study the Sun-shadow dynamics, it is useful to construct a Poincaré map. Traditionally, the Poincaré maps of autonomous two-dimensional Hamiltonian systems are defined by fixing the value of the Hamiltonian. This is not possible for the Sun-shadow dynamics, since the Hamiltonian is not conserved along the flow, see Proposition 2. However, here we can fix the value of $\mathscr{L}_s$. Indeed, even though $\mathscr{L}_s$ is not a constant of motion as well, it assumes the same value in Stark's regime before and after the satellite crosses the shadow. To define a Poincaré map we also need to introduce a section. The selected section corresponds to the upper boundary of the shadow region in the (x, y) configuration space, i.e. to $y = R$, $x \geq 0$. We consider trajectories leaving the section with $p_y > 0$, in the outward direction with respect to the shadow region. Since the dependence on the coordinates is decoupled in the variables u, v (see (17), (18)), we decided to use them to define the map. Thus, we define the Sun-shadow map as

$$\mathfrak{S} : \mathcal{D} \subset \mathbb{R}^2 \to \mathbb{R}^2,$$
$$(u, p_u) \mapsto (u', p_u'),$$

where the domain $\mathcal{D}$ is discussed below, and $(u, p_u), (u', p_u')$ belong to the section Σ defined as

$$\Sigma = \{(p_u, p_v, u, v) :\ |u| \geq \sqrt{R},\ uv = R,\ up_v > \max(0, -p_u v),\ \mathscr{L}_s = \ell_s\}.$$

The conditions $|u| \geq \sqrt{R}$, $uv = R$ are necessary to select the desired section in the (x, y) configuration space. The condition $up_v > -p_u v$ is equivalent to $p_y > 0$ (see (8)). The additional condition, $up_v > 0$, assures that every point $(u, p_u) \in \Sigma$ corresponds to only one trajectory. Indeed, there are points (u, p_u) for which $p_y > 0$ in both the cases $p_v > 0$ and $p_v < 0$.

Proposition 4. *The map $\mathfrak{S}$ is not defined in the points (u, p_u) with*

$$p_u^2 \leq 2(\mu+\ell_s) + fR^2 + (f - 2(\mu-\ell_s)/R^2)u^4. \tag{54}$$

Moreover, in the second and the fourth quadrant of the (u, p_u) plane $\mathfrak{S}$ is not defined if $\ell_s > \mu - \frac{fR^2}{2}$, while if $\ell_s < \mu - \frac{fR^2}{2}$ it is not defined only in the points (u, p_u) with

$$u^4 \leq \frac{2(\mu+\ell_s)+fR^2}{2(\mu-\ell_s)-fR^2}R^2. \tag{55}$$

Proof. For each point (u, p_u) in the domain of the map, we have

$$v = \frac{R}{u}, \tag{56}$$

and p_v is defined by $(18)_2$. Condition (54) corresponds to $p_v^2 \leq 0$, that is not possible. In the second and the fourth quadrant of the (u, p_u) plane, the condition $up_v > \max(0, -p_u v)$ with the constraint (56) results in

$$p_v u > -p_u\frac{R}{u},$$

which implies

$$\left(2(\mu-\ell_s) - fR^2\right)u^4 - 2(\mu+\ell_s)R^2 - fR^4 > 0. \tag{57}$$

If $\ell_s > \mu - \frac{fR^2}{2}$, we get

$$u^4 < \frac{2(\mu+\ell_s)+fR^2}{2(\mu-\ell_s)-fR^2}R^2 < 0,$$

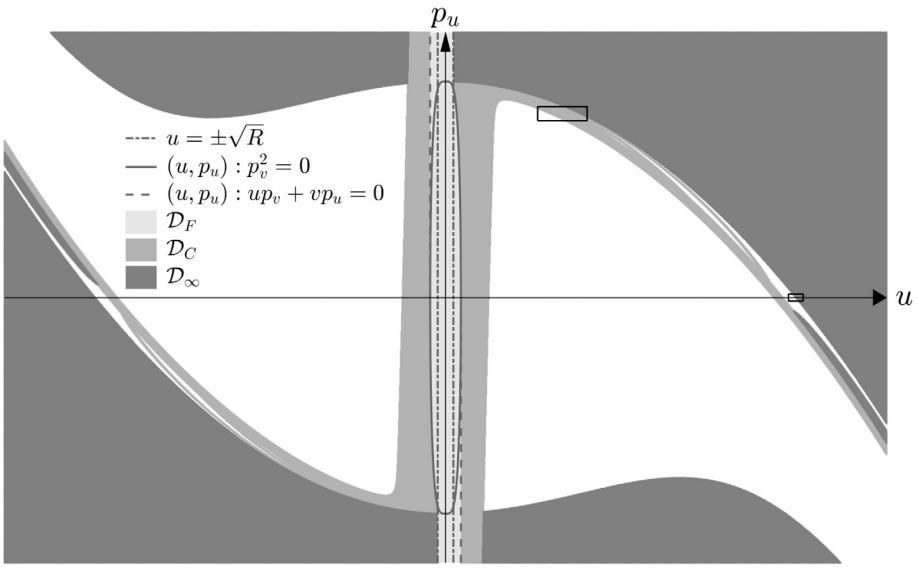

Fig. 9. The domain $\mathcal{D}$ of the Sun-shadow map is represented by the white area. Here $\ell_s = 348\,600$ km^3/s^2, $f = 9.12 \times 10^{-9}$ km/s^2. A magnification of the region in the small and smaller rectangles is shown in Figs. 11 and 12, respectively.

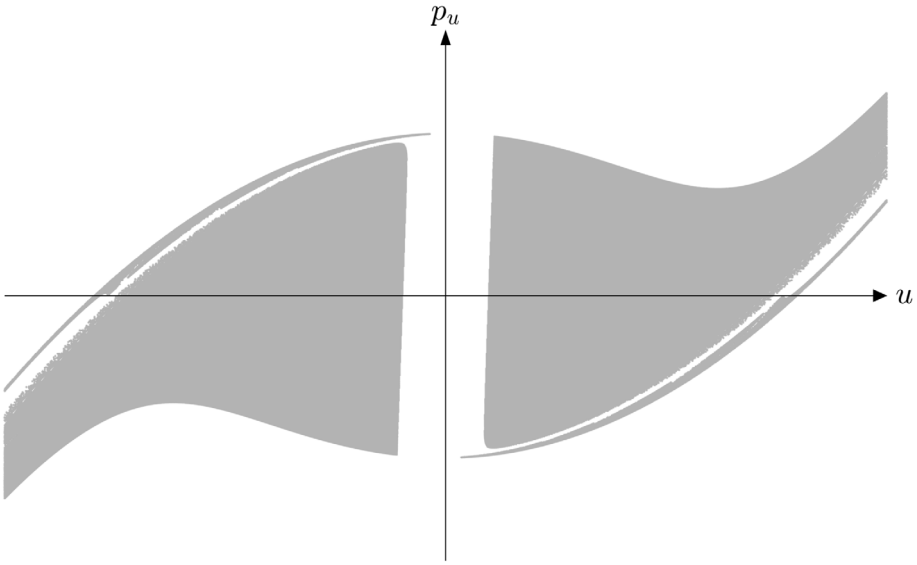

Fig. 10. The image of the Sun-shadow map.

meaning that the map is not defined. On the other hand, if $\ell_s < \mu - \frac{fR^2}{2}$, condition (57) is fulfilled for

$$u^4 > \frac{2(\mu + \ell_s) + fR^2}{2(\mu - \ell_s) - fR^2} R^2. \quad \square$$

The domain $\mathcal{D} \subset \mathbb{R}^2$ does not include the points defined in Proposition 4, nor the points corresponding to trajectories which go to infinity or collide with the Earth before going back to Σ. In Fig. 9, for a specific choice of ℓ_s and f, the domain $\mathcal{D}$ is drawn as the white area in a portion of the (u, p_u) plane. The light grey region represents the set $\mathcal{D}_F$ of forbidden points in Proposition 4. The other two grey areas contain part of the sets $\mathcal{D}_\infty$ (darker) and $\mathcal{D}_C$ (lighter) corresponding to the trajectories which go to infinity and collide with the Earth, respectively.

Fig. 10 shows the image of the domain $\mathcal{D}$ under $\mathfrak{S}$ in the same portion of the (u, p_u) plane represented in Fig. 9.

Remark 6. In the image of the map we may have points belonging to $\mathcal{D}_\infty$ or $\mathcal{D}_C$, so that we cannot iterate the map again.

In Fig. 11, the magnification of the larger rectangular region appearing in Fig. 9 highlights the complexity of the structure of $\mathcal{D}$. We have selected five points, labelled with b, c, d, e, f, in the white *corridors*, and one point, labelled with a, in the larger white region on the left. In the same figure we show the portion of the trajectories corresponding to one iteration of the selected points under the map. A winding number around the origin can be associated to each trajectory by joining with a straight line their initial and final points. The values of this topological invariant are -4, -3, -2, -1, 0, $+1$ for the cases (b), (c), (d), (e), (f), (a), respectively. Since we get a different value for all these cases, the white corridors must belong to different connected components of $\mathcal{D}$.

Proposition 5. *The map $\mathfrak{S}$ is differentiable in its definition domain $\mathcal{D}$.*

Proof. Let $\boldsymbol{\Phi}_s(\tau; \boldsymbol{U}, \tau_0)$ and $\boldsymbol{\Phi}_k(\tau; \boldsymbol{U}, \tau_0)$ be the integral flow of Stark's and Kepler's dynamical systems (11), (12). Consider

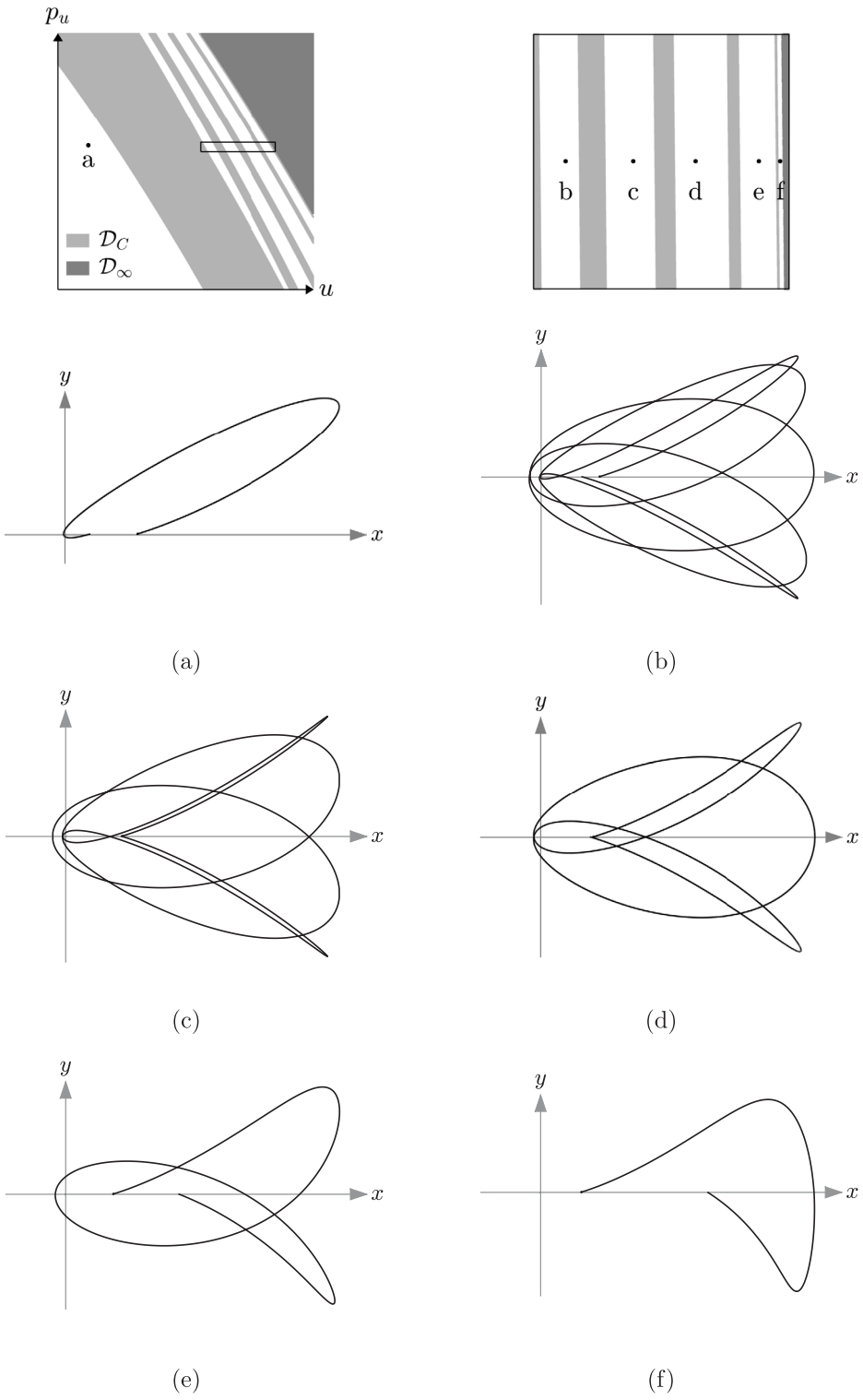

Fig. 11. Orbits with different winding numbers, corresponding to one iteration of $\mathfrak{S}$. The selected initial points are shown in the two top pictures and are labelled with a, b, c, d, e, f. On top right there is the magnification of the small rectangular region on top left.

$(u, p_u) \in \mathcal{D}$ and the corresponding orbit in the Sun-shadow dynamics. Before it goes back to the section Σ, the dynamical regime will change n times, with n depending on the shape of the trajectory. The first regime will be always Stark's, the last will be Kepler's. Let us introduce a finite sequence of sections Σ_i, $i = 0, \dots, n$ where the dynamics changes, with $\Sigma_0 = \Sigma_n = \Sigma$. Each of them is given by $s_i(\boldsymbol{U}) = 0$: for the section Σ we have $s_i = uv - R$, while for the intermediate sections, with $i = 1, \dots, n-1$, we have $s_i = uv + R$ or $s_i = uv - R$ depending on the boundary of the shadow region that is crossed when the dynamics changes. It

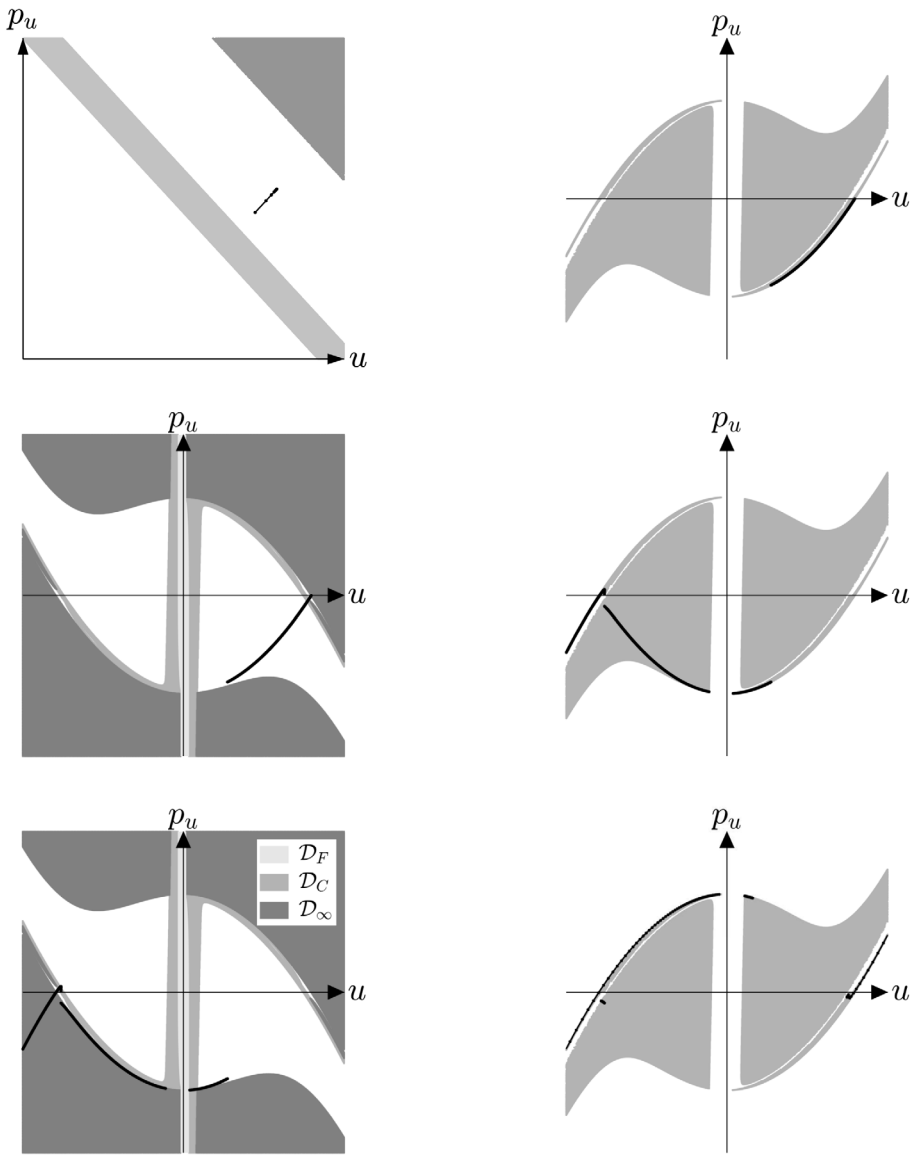

Fig. 12. Constructing one branch of the unstable manifold of $\widehat{\boldsymbol{v}}_1$. In the background there are the domain $\mathcal{D}$ and the forbidden regions $\mathcal{D}_F, \mathcal{D}_C, \mathcal{D}_\infty$ (left), the image of the map $\mathfrak{S}(\mathcal{D})$ (right). The initial primary, drawn in the top left figure, is located in the smaller rectangle in Fig. 9. Here, $\ell_s = 348\,600$ km^3/s^2, $f = 9.12 \times 10^{-9}$ km/s^2.

is possible to define the maps

$$\begin{aligned} &\mathfrak{S}_i : \mathcal{D}_i \subset \mathbb{R}^2 \to \mathbb{R}^2, \\ &\qquad (u^i, p_u^i) \mapsto (u^{i+1}, p_u^{i+1}), \end{aligned} \tag{58}$$

where $\mathcal{D}_i$ is made of the points

$$\boldsymbol{U}_i = (p_u^i, p_v^i, u^i, v^i)^T \in \Sigma_i, \qquad v^i = \pm R/u^i, \qquad p_v^i = p_v(u^i, p_u^i).$$

The Sun-shadow map will be given by

$$\mathfrak{S} = \mathfrak{S}_{n-1} \circ \ldots \circ \mathfrak{S}_1 \circ \mathfrak{S}_0.$$

Thus, we have

$$\begin{aligned} D\mathfrak{S}(u, p_u) &= \frac{\partial(u', p_u')}{\partial(u, p_u)} \\ &= \frac{\partial(u', p_u')}{\partial(u^{n-1}, p_u^{n-1})} \frac{\partial(u^{n-1}, p_u^{n-1})}{\partial(u^{n-2}, p_u^{n-2})} \cdots \frac{\partial(u^2, p_u^2)}{\partial(u^1, p_u^1)} \frac{\partial(u^1, p_u^1)}{\partial(u, p_u)} \end{aligned} \tag{59}$$

where

$$\begin{aligned} \frac{\partial(u^{i+1}, p_u^{i+1})}{\partial(u^i, p_u^i)} = A\Big(\boldsymbol{X}_{i+1}(\boldsymbol{U}_{i+1}) \frac{\partial \tau}{\partial \boldsymbol{U}_i} + \frac{\partial \boldsymbol{\Phi}_{i+1}}{\partial \boldsymbol{U}_i}(\tau(\boldsymbol{U}_i); \boldsymbol{U}_i, \tau_i)\Big) \\ \times \frac{\partial \boldsymbol{U}_i}{\partial(u^i, p_u^i)}, \end{aligned}$$

with

$$A = \begin{bmatrix} 0 & 0 & 1 & 0 \\ 1 & 0 & 0 & 0 \end{bmatrix}.$$

The integral flow $\boldsymbol{\Phi}_{i+1}$ (resp. $\boldsymbol{X}_{i+1}$) is equal to either $\boldsymbol{\Phi}_s$ or $\boldsymbol{\Phi}_k$ (resp. $\boldsymbol{X}_s$ or $\boldsymbol{X}_k$) depending on the regime between the two sections. The term $\partial \tau / \partial \boldsymbol{U}_i$ can be computed as

$$\frac{\partial \tau}{\partial \boldsymbol{U}_i} = -\frac{1}{\frac{\partial s_{i+1}}{\partial \boldsymbol{U}}(\boldsymbol{U}_{i+1}) \boldsymbol{X}_{i+1}(\boldsymbol{U}_{i+1})} \frac{\partial s_{i+1}}{\partial \boldsymbol{U}}(\boldsymbol{U}_{i+1}) \frac{\partial \boldsymbol{\Phi}_{i+1}}{\partial \boldsymbol{U}_i}(\tau(\boldsymbol{U}_i); \boldsymbol{U}_i, \tau_i),$$

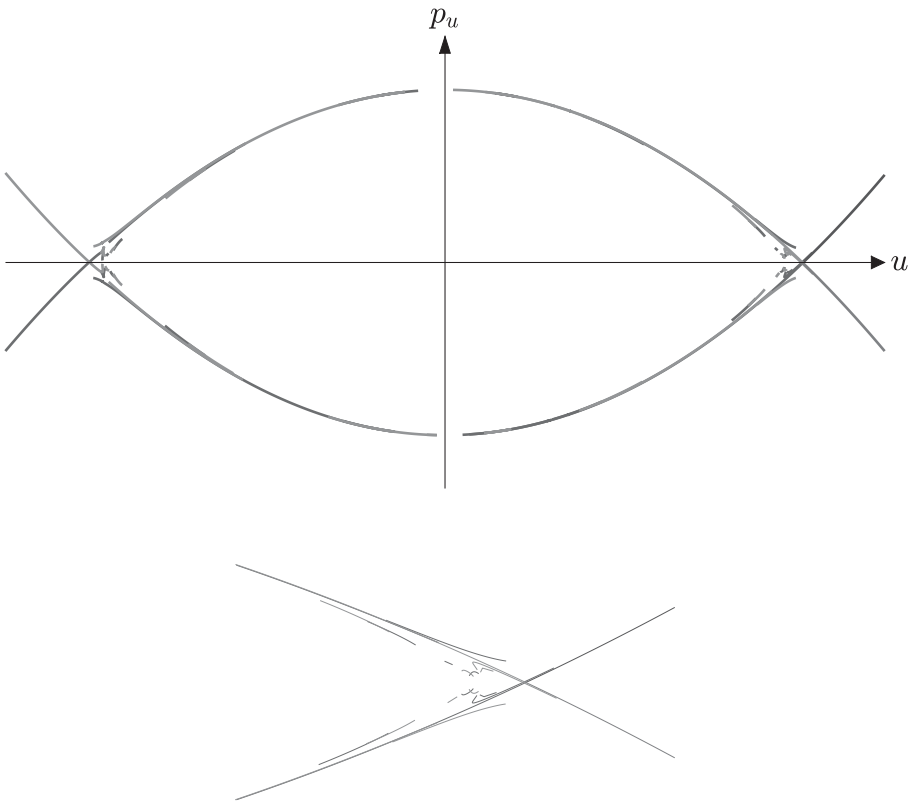

Fig. 13. Stable and unstable invariant manifolds of $\widehat{\boldsymbol{v}}_1$. At the bottom we zoom in the region close to $\widehat{\boldsymbol{v}}_1$. Note that the branches of the manifolds are made by several connected components.

see [16], while $\partial \boldsymbol{\Phi}_{i+1}/\partial \boldsymbol{U}_i$ fulfils

$$\frac{d}{d\tau}\Big(\frac{\partial \boldsymbol{\Phi}_{i+1}}{\partial \boldsymbol{U}_i}(\tau(\boldsymbol{U}_i);\boldsymbol{U}_i,\tau_i)\Big) = \frac{\partial \boldsymbol{X}_{i+1}}{\partial \boldsymbol{U}}\Big(\boldsymbol{\Phi}_{i+1}(\tau(\boldsymbol{U}_i);\boldsymbol{U}_i,\tau_i)\Big)\frac{\partial \boldsymbol{\Phi}_{i+1}}{\partial \boldsymbol{U}_i}(\tau(\boldsymbol{U}_i);\boldsymbol{U}_i,\tau_i),$$

$$\frac{\partial \boldsymbol{\Phi}_{i+1}}{\partial \boldsymbol{U}_i}(\tau_i;\boldsymbol{U}_i,\tau_i) = I,$$

with I the identity matrix and τ_i the value of the fictitious time at the section Σ_i. □

5.1. Non-preservation of area

The map $\mathfrak{S}$ is not area-preserving. We give numerical evidence by showing that a circular region of Σ is mapped into a region with a different area. In the section Σ, we can consider a closed curve γ_0 symmetric with respect to the u axis, defined by

$$c\,p_u^2 + (u-u_C)^2 = r_C^2,$$

with

$$u_C > r_C + \Big(\frac{2(\mu+\ell_s)+fR^2}{2(\mu-\ell_s)-fR^2}R^2\Big)^{\frac{1}{4}}.$$

We have $c = 1\ \mathrm{s}^2/\mathrm{km}^2$ so that γ_0 becomes a circumference of radius r_C centred at $(u,p_u) = (u_C,0)$. We sample it with m points. Each point defines a trajectory in the phase space that we propagate with a Runge–Kutta method of Gauss type, by properly switching dynamics at the boundary between Stark's and Kepler's regimes, until its next intersection with the section Σ. In this way, we obtain the image of the initial points under the Sun-shadow map. The resulting points belong to the closed curve $\gamma_1 = \mathfrak{S}(\gamma_0)$. To compute the area A_1 of the region $\mathcal{A}_1$ enclosed by γ_1, first we parametrise it by a variable θ. In particular, for each point on γ_1 we compute the values of the parameter θ:

$$\theta^1 = 0; \qquad \theta^j = \theta^{j-1} + \sqrt{(p_u^j - p_u^{j-1})^2 + (u^j - u^{j-1})^2},$$
$$j = 2,\dots,m,$$

where (u^j, p_u^j) are the coordinates of the points, and $(u^m, p_u^m) = (u^1, p_u^1)$. Then, we interpolate the points $(\theta^j, u^j), (\theta^j, p_u^j)$ by cubic splines. Finally, we compute the area by applying the Gauss–Green formula

$$\int_{\mathcal{A}_1} du dp_u = \frac{1}{2}\int_{\gamma_1} -p_u du + u dp_u,$$

and we get

$$A_1 = \sum_{j=1}^{m-1}\frac{1}{2}\int_{\theta_j}^{\theta_{j+1}}\Big(-p_u(\theta)\frac{du}{d\theta}(\theta) + u(\theta)\frac{dp_u}{d\theta}(\theta)\Big)d\theta.$$

The resulting area A_1 is different from the area $A_0 = \pi r_C^2/\sqrt{c}$ of the region enclosed by γ_0. Indeed, assuming that

$$\ell_s = 348600\ \mathrm{km}^3/\mathrm{s}^2, \quad f = 9.12\times10^{-9}\ \mathrm{km}/\mathrm{s}^2,$$
$$u_C = 1250\ \mathrm{km}^{1/2}, \quad r_C = 250\ \mathrm{km}^{1/2},$$

and sampling the initial circumference with 2×10^5 points, in double precision we get

$$A_0 \approx 1.9635\times10^5\ \mathrm{km}^2/\mathrm{s}, \qquad A_1 \approx 1.9588\times10^5\ \mathrm{km}^2/\mathrm{s}.$$

5.2. Hyperbolic fixed points

Given $\ell_s \in [\ell_s^-, \ell_s^+]$, the periodic orbit of brake type $\widehat{\boldsymbol{x}}(t;\ell_s)$ gives rise to two fixed points $\widehat{\boldsymbol{v}}_{1,2}$ of the Sun-shadow map:

$$\widehat{\boldsymbol{v}}_1 = (\sqrt{\xi_E}, -p_{u_E}), \qquad \widehat{\boldsymbol{v}}_2 = (-\sqrt{\xi_E}, p_{u_E}),$$

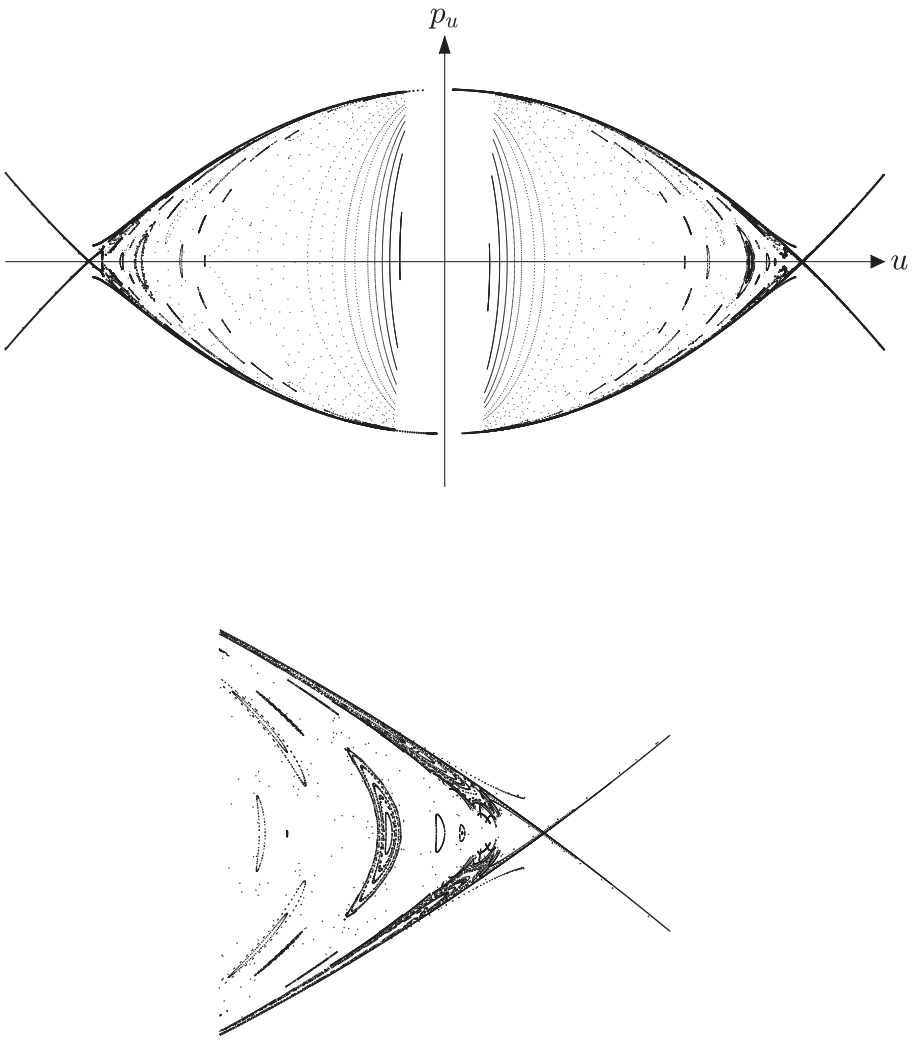

Fig. 14. On the top we show a global picture of the Sun-shadow map, with $\ell_s = 348\,600$ km^3/s^2, $f = 9.12 \times 10^{-9}$ km/s^2. At the bottom we zoom in the region close to $\widehat{\boldsymbol{v}}_1$.

where ξ_E is given by Eq. (36) and

$$p_{u_E}^2 = 2\widehat{h}_s\xi_E + 2(\mu + \ell_s) + f\xi_E^2, \qquad p_{u_E} > 0,$$

with $\widehat{h}_s$ the energy of $\widehat{\boldsymbol{x}}$ in Stark's regime, $\widehat{h}_s \in [\bar{h}_s, h_s^*)$. The point $\widehat{\boldsymbol{v}}_1$ lies in the region included into the smaller rectangle appearing in Fig. 9.

We can evaluate the Jacobian matrix of the map at $\widehat{\boldsymbol{v}}_j$, $j = 1, 2$, using Eq. (59): it has two real eigenvalues λ_1^j, λ_2^j with

$$0 < \lambda_1^j < 1 < \lambda_2^j.$$

For example, by taking $\ell_s = 348\,600$ km^3/s^2, we obtain $\lambda_1^j = 1.54 \times 10^{-4}$ and $\lambda_2^j = 6.48 \times 10^3$, for $j = 1, 2$. Thus, the two fixed points are hyperbolic. It follows that the periodic orbit of brake type is unstable.

5.3. Invariant manifolds

Here, we describe the numerical technique used for the computation of the invariant manifolds of the fixed points of the Sun-shadow map. The discussion will be focused on $\widehat{\boldsymbol{v}}_1$, but the procedure is the same also for $\widehat{\boldsymbol{v}}_2$.

We took inspiration from the method in [17], thought specifically for planar maps. This algorithm can be applied only to two-dimensional maps which have saddle-type fixed points and whose Jacobian matrix, evaluated at these points, has two real eigenvalues λ_1, λ_2 with $0 < \lambda_1 < 1 < \lambda_2$. As previously shown, the Sun-shadow map $\mathfrak{S}$ and its fixed point $\widehat{\boldsymbol{v}}_1$ fulfil these requirements. We describe the algorithm for the case of one branch B of the unstable manifold. The stable manifold can be constructed in a similar manner using the inverse map $\mathfrak{S}^{-1}$. The method consists in dividing the branch of the manifold into a sequence of primary segments. A primary segment V is a connected subset of B whose last point is the image of its first point under the map. Given an initial primary (segment) V_0 in a neighbourhood of the fixed point, all the following primaries can be obtained by iterating the map m times:

$$V_{i+1} = \mathfrak{S}(V_i), \qquad i = 0, \dots, m-1.$$

The branch will be given by the union of the computed primaries:

$$B = \bigcup_i V_i.$$

The initial primary is approximated with a segment very close to $\widehat{\boldsymbol{v}}_1$ along an unstable eigenvector $\boldsymbol{\psi}$ of $D\mathfrak{S}(\widehat{\boldsymbol{v}}_1)$. Then, it is corrected by using the technique described in [18, Section 2.2], based on the Modified Fast Lyapunov Indicators (MFLI). Through a suitable windowing, the MFLI allow to compute the invariant manifolds also when the traditional FLI fail, see [19]. The lower is the distance of a point from the manifold, the larger is its MFLI.

Table 2
Stark's problem: boundaries of the four regions in the $(\ell_s, h_s/\sqrt{f})$ plane. The features of the trajectories in the (x, y) plane are qualitatively described. i is the imaginary unit.

Regions *I*, *II*	$\ell_s = -\mu$; $h_s/\sqrt{f} \in (0, +\infty)$
$V(v)$, $U(u)$ roots v, u variable Trajectories type	$v_1 > 0$, $v_2 \in i\mathbb{R}$, $u_1 = 0$, $u_2 \in i\mathbb{R}$ $v \in [-v_1, v_1]$, $u \in (-\infty, +\infty)$ Two types: periodic, brake, passing through the origin; asymptotic to the periodic orbit in the future or in the past
Regions *I*, *IV*	$\ell_s = -\mu$; $h_s/\sqrt{f} \in (-\infty, 0)$
$V(v)$, $U(u)$ roots v, u variable Trajectories type	$v_1 > 0$, $v_2 \in i\mathbb{R}$, $u_1 > u_2 = 0$ $v \in [-v_1, v_1]$, $u \in (-\infty, -u_1] \cup \{0\} \cup [u_1, +\infty)$ Two types: brake, periodic, passing through the origin; unbounded, self-intersecting, not encircling the origin
Regions *II*, *IV*	$\ell_s = (-\mu, \mu)$; $h_s/\sqrt{f} = -\sqrt{2(\mu + \ell_s)}$
$V(v)$, $U(u)$ roots v, u variable Trajectories type	$v_1 > 0$, $v_2 \in i\mathbb{R}$, $u_1 = u_2$, $u_1, u_2 > 0$ $v \in [-v_1, v_1]$, $u \in (-\infty, +\infty)$ Two types: periodic, brake; asymptotic to the periodic orbit in the future or in the past
Regions *II*, *III*	$\ell_s = \mu$; $h_s/\sqrt{f} \in (0, +\infty)$
$V(v)$, $U(u)$ roots v, u variable Trajectories type	$v_1 > v_2 = 0$, $u_1, u_2 \in \mathbb{C} \setminus \mathbb{R}$ $v \in [-v_1, v_1]$, $u \in (-\infty, +\infty)$ Two types: unbounded, not self-intersecting; unbounded with $y = 0$ and $x \geq 0$
Region *II*	$\ell_s = \mu$; $h_s/\sqrt{f} \in (-\sqrt{2(\mu + \ell_s)}, 0)$
$V(v)$, $U(u)$ roots v, u variable Trajectories type	$v_1 = 0$, $v_2 \in i\mathbb{R}$, $u_1, u_2 \in \mathbb{C} \setminus \mathbb{R}$ $v = 0$, $u \in (-\infty, +\infty)$ Unbounded with $y = 0$ and $x \geq 0$
Region *IV*	$\ell_s = \mu$; $h_s/\sqrt{f} \in (-\infty, -\sqrt{2(\mu + \ell_s)})$
$V(v)$, $U(u)$ roots v, u variable Trajectories type	$v_1 = 0$, $v_2 \in i\mathbb{R}$, $u_1 > u_2 > 0$ $v = 0$, $u \in (-\infty, -u_1] \cup [-u_2, u_2] \cup [u_1, +\infty)$ Two types: brake, periodic, passing through the origin; unbounded, with $y = 0$, $x > 0$
Region *III*	$\ell_s \in (\mu, +\infty)$; $h_s/\sqrt{f} = \sqrt{-2(\mu - \ell_s)}$
$V(v)$, $U(u)$ roots v, u variable Trajectories type	$v_1 = v_2$, $v_1, v_2 > 0$, $u_1, u_2 \in \mathbb{C} \setminus \mathbb{R}$ $v \in \{\pm v_1\}$, $u \in (-\infty, +\infty)$ Unbounded, not self-intersecting, parabolic

Thus, for each point $\boldsymbol{v}$ in the sample of the primary (see below) the correction is done as follows:

1. consider a small neighbourhood of $\boldsymbol{v}$ in the direction orthogonal to the corresponding primary curve, and sample it uniformly;
2. compute the MFLI of $\boldsymbol{v}$ and of each point of the sample;
3. select the point with the largest MFLI.

There is an issue concerning the iterations of the primaries. We observed that, after a few iterations, portions of the primaries are lost because the corresponding trajectories never return to Σ: by consequence the primaries lose their nature of connected sets. We decided to relax the definition of primaries given by Hobson by admitting primaries with several connected components, that we still denote by V_i.

We summarise below our algorithm:

1. take an approximate sampling of the initial primary V_0 in a small neighbourhood of $\widehat{\boldsymbol{v}}_1$ as follows: consider $n-1$ points aligned with the eigenvector $\boldsymbol{\psi}$ distributed according to the exponential law

$$\boldsymbol{v}_i = \boldsymbol{v}_{i-1} + a\, 2^i\, \boldsymbol{\psi}, \qquad i = 1, \ldots, n-2,$$

with $\boldsymbol{v}_i = (u_i, p_{u_i})$ and $a \in \mathbb{R}$. As the last point of the sampling, $\boldsymbol{v}_{n-1}$, take the image of $\boldsymbol{v}_0$ under the map. We call $\tilde{V}_0$ the finite set of points approximating V_0;
2. correct $\tilde{V}_0$ by using the MFLI, as previously described;
3. iterate the corrected $\tilde{V}_0$ once, and obtain the set

$$\tilde{V}_1 = \{\boldsymbol{v}'_i = (u'_i, p'_{u_i}),\ i = 0, \ldots, n-1\};$$

4. interpolate the points in $\tilde{V}_1$ with cubic splines and sample more densely the resulting curve (we still denote by $\tilde{V}_1$ the new sample);
5. correct $\tilde{V}_1$ by the MFLI, as done for $\tilde{V}_0$;
6. iterate the corrected $\tilde{V}_1$ under the map $m-1$ times.

Fig. 12 shows the first steps of the construction of a branch of the unstable manifold. The initial primary V_0 (top left) is first iterated once under the map (top right). Its image V_1 intersects the forbidden region $\mathcal{D}_C$ (middle left), and at the second iteration of $\mathfrak{S}$ three components are left (middle right), two of which lie in the $\{u < 0\}$ half-plane. Again, their image V_2 intersects the forbidden regions $\mathcal{D}_C$, $\mathcal{D}_\infty$ (bottom left) and the number of components increases at the successive iteration (bottom right).

In Fig. 13 we draw the four (disconnected) branches of the stable and unstable manifolds of the fixed point $\widehat{\boldsymbol{v}}_1$.

6. Conclusions and open questions

In this paper we have investigated the Sun-shadow dynamics, which is defined by patching together Kepler's and Stark's dynamics. After reviewing some relevant features of Stark's problem, we prove the existence of a family of periodic orbits of brake type. Then, we introduce the Sun-shadow map, by fixing a quantity which is not conserved along the flow. This map is differentiable but is not area preserving. Its domain shows fine structures that underlie interesting phenomena when the map is iterated many times. There is numerical evidence that the fixed points $\widehat{\boldsymbol{v}}_1$, $\widehat{\boldsymbol{v}}_2$ related to the periodic orbits of brake type are hyperbolic; their invariant manifolds are constructed by an algorithm specifically created for this purpose. A global picture of

Table 3
Stark's problem: boundary points in the $(\ell_s, h_s/\sqrt{f})$ plane. The features of the trajectories in the (x, y) plane are qualitatively described. i is the imaginary unit.

Regions *I*, *II*, *IV*	$\ell_s = -\mu$; $h_s/\sqrt{f} = 0$
$V(v)$, $U(u)$ roots	$v_1 > 0$, $v_2 = 0$, $u_1 = 0$, $u_2 \in i\mathbb{R}$
v, u variable	$v \in [-v_1, v_1]$, $u \in (-\infty, +\infty)$
Trajectories type	Two types: periodic, brake, passing through the origin; asymptotic to the periodic orbit in the future and in the past
Regions *II*, *III*	$\ell_s = \mu$; $h_s/\sqrt{f} = 0$
$V(v)$, $U(u)$ roots	$v_1 = 0$, $v_2 = 0$, $u_1, u_2 \in \mathbb{C} \setminus \mathbb{R}$
v, u variable	$v = 0$, $u \in (-\infty, +\infty)$
Trajectories type	Unbounded with $y = 0$ and $x \geq 0$
Regions *II*, *IV*	$\ell_s = \mu$; $h_s/\sqrt{f} = -\sqrt{2(\mu + \ell_s)}$
$V(v)$, $U(u)$ roots	$v_1 = 0$, $v_2 \in i\mathbb{R}$, $u_1 = u_2$, $u_1, u_2 > 0$
v, u variable	$v = 0$, $u \in (-\infty, +\infty)$
Trajectories type	Fixed point; asymptotic to the fixed point in the future and in the past with $y = 0$, $x \geq 0$

this map is drawn in Fig. 14, where an enhancement of the region close to the point $\widehat{\boldsymbol{v}}_1$ is also displayed. We observe evidence of regular and chaotic behaviour, with the presence of several islands: we checked that some of them surround periodic points. In the central region, where we have smaller values of $|u|$, the plotted points show a regular structure, similar to the one of the phase portrait in Fig. 3. On the other hand, the regular behaviour seems to be lost in a neighbourhood of $\widehat{\boldsymbol{v}}_1$, along the stable and unstable branches of its invariant manifold.

This study opens some interesting questions about the Sun-shadow dynamics, which deserve to be further investigated. First, we may wonder whether the winding number associated to the trajectories corresponding to one iteration of the map is bounded from below, see Fig. 11. Another interesting question is whether we can show that the islands appearing in Fig. 14 correspond to invariant curves around fixed or periodic points. Moreover, we can ask ourselves whether Melnikov's method can be adapted to prove the existence of chaotic dynamics in this case, where the invariant manifolds of the fixed points $\widehat{\boldsymbol{v}}_1$, $\widehat{\boldsymbol{v}}_2$ are made of several connected components (maybe infinitely many) due to the presence of the forbidden regions $\mathcal{D}_\infty$, $\mathcal{D}_C$, see Fig. 12. Finally, possible future developments of this work are the extension of the Sun-shadow dynamics to the three-dimensional case, the inclusion of other perturbations (e.g. the Earth oblateness), and the study of the effect of the penumbra.

CRediT authorship contribution statement

Irene Cavallari: Conceptualization, Methodology, Writing – original draft. **Giovanni F. Gronchi:** Conceptualization, Methodology, Writing – original draft. **Giulio Baù:** Conceptualization, Methodology, Writing – original draft.

Declaration of competing interest

The authors declare that they have no known competing financial interests or personal relationships that could have appeared to influence the work reported in this paper.

Acknowledgements

The authors have been partially supported through the H2020 MSCA ETN Stardust-Reloaded, Grant Agreement No. 813644. GFG and GB also acknowledge the project MIUR-PRIN 20178CJA2B "New frontiers of Celestial Mechanics: theory and applications", and the GNFM-INdAM (Gruppo Nazionale per la Fisica Matematica).

Appendix

See Tables 2 and 3.

References

[1] P. Musen, The influence of the solar radiation pressure on the motion of an artificial satellite, J. Geophys. Res. 65 (5) (1960) 1391–1396.
[2] R.W. Parkinson, H.M. Jones, I.I. Shapiro, Effects of solar radiation pressure on earth satellite orbits, Science 131 (3404) (1960) 920–921.
[3] A. Milani, A.A. Nobili, P. Farinella, Non-Gravitational Perturbations and Satellite Geodesy, IOP Publishing, Bristol, 1987.
[4] Y. Kozai, Effects of the solar-radiation pressure on the motion of an artificial satellite, Smithsonian Contrib. Astrophys. 6 (1960) 109–112.
[5] M.L. Lidov, Secular effects in the evolution of orbits under the influence of radiation pressure, Transl. Kosmicheskie Issledovaniya 7 (4) (1969) 467–484.
[6] S. Ferraz Mello, Analytical study of the Earth's shadowing effects on satellite orbits, Celestial Mech. 5 (1972) 80–101.
[7] C. Hubaux, A. Lemaître, The impact of Earth's shadow on the long-term evolution of space debris, Celestial Mech. Dynam. Astronom. 116 (2013) 79–95.
[8] C. Hubaux, A.-S. Libert, N. Delsate, T. Carletti, Influence of Earth's shadowing effects on space debris stability, Adv. Space Res. 51 (2013) 25–38.
[9] V.V. Beletski, Essays on the Motion of Celestial Bodies, Springer, Basel, 2001.
[10] V.V. Beletski, Space-flight trajectories with a constant-reaction accelerator vector, Transl. Kosmicheskie Issledovaniya 2 (3) (1964) 408–413.
[11] G. Baú, A. Celletti, C. Galeş, G.F. Gronchi, Satellite Dynamics and Space Missions, Springer, 2019.
[12] P.J. Redmond, Generalization of the Runge-Lenz vector in the presence of an electric field, Phys. Rev. 133 (5) (1964) 1352–1353.
[13] H. Goldstein, Classical Mechanics, Addison-Wesley publishing company, 1950.
[14] E.L. Stiefel, G. Scheifele, Linear and Regular Celestial Mechanics, Springer–Verlag, 1971.
[15] D.A. Cox, The arithmetic-geometric mean of Gauss, L'Enseign. Math. 30 (1984) 275–330.
[16] C. Simó, On the analytical and numerical approximation of invariant manifolds, in: E. Frontières (Ed.), Modern Method in Celestial Mechanics, Benest, D., Froeschle, C., Observatoire de la Côte d'azur, 1989, pp. 285–329.
[17] D. Hobson, An efficient method for computing invariant manifolds of planar maps, J. Comput. Phys. 104 (1993) 14–22.
[18] E. Lega, M. Guzzo, Three-dimensional representations of the tube manifolds of the planar restricted three-body problem, Physica D 325 (2016) 41–52.
[19] E. Lega, M. Guzzo, Evolution of the tangent vectors and localization of the stable and unstable manifolds of hyperbolic orbits by Fast Lyapunov indicators, J. Appl. Math. 74 (4) (2014) 1058–1086.